Characterization of the Fast Dynamics of Protein Amino Acid Side Chains Using NMR Relaxation in Solution

Tatyana I. Igumenova,[†] Kendra King Frederick, and A. Joshua Wand*

Johnson Research Foundation and Department of Biochemistry & Biophysics, University of Pennsylvania, Philadelphia, Pennsylvania 19104-6059

Contents

1. Introduction

The physical basis of protein structure, dynamics, and function has been intensely studied for several decades. Indeed, since the new millennium, there has been a tremendous expansion in the number of unique topological folds that have been characterized at high resolution by crystallographic and nuclear magnetic resonance (NMR) based methods. In the midst of this rush toward a grand scale structural genomics effort, a quieter effort dedicated to the experimental characterization of protein conformational heterogeneity has also emerged. The influence of atomic scale structure on molecular recognition and catalysis by proteins is often the focus of attention while the role of dynamics is largely unknown and frequently ignored. Nevertheless, it has long been recognized that proteins are indeed dynamic systems. Early insights into the time scale and character of protein internal motion largely employed local optical probes, unresolved hydrogen exchange, and one-dimensional NMR techniques that, though limited, revealed a startling complexity and richness in the internal motion of proteins.[1–5] These initial views contributed significantly to the development of current treatments of protein dynamics and thermodynamics.[6] The connection to biological function rather than just biological form is more recent. Internal protein dynamics can potentially affect protein function through a variety of mechanisms, some of which are tautological or obvious in nature while others are subtle and remain to be fully explored and appreciated. There are now several examples of protein–protein and protein–ligand interactions that illustrate that dynamics may be fundamentally linked to function in several ways. NMR spectroscopy is very much at the center of current efforts to illuminate the nature of protein dynamics and their role in biological function. Here we will focus on the use of solution NMR methods to provide fast sub-nanosecond dynamics of protein side chains. The interested reader is referred to separate reviews in this issue by Jarymowycz and Stone,[7] Tolman and Ruan,[8] and Palmer and Massi[9] discussing dynamics of the polypeptide backbone.

* To whom correspondence should be addressed. Telephone: 215-573-7288. Fax: 215-573-7290. E-mail: wand@mail.med.upenn.edu.
† Present address: Department of Biochemistry & Biophysics, Columbia University, New York, NY 10032.

Tatyana Igumenova was born and raised in Novosibirsk, Russia. She completed her undergraduate degree in chemistry at Novosibirsk State University. In 2003, she received her Ph.D. (with distinction) in chemistry from Columbia University for work with Ann McDermott on solid-state NMR of proteins. From 2003 to 2005, she was an NIH postdoctoral fellow with Josh Wand at the University of Pennsylvania, where she studied the role of fast side chain dynamics in long-range coupling of allosteric sites in calmodulin. She is currently an NIH postdoctoral fellow with Arthur G. Palmer, III, at Columbia University.

Kendra K. Frederick received her B.S. in French language and literature and biochemistry with honors in 2000 from the University of Michigan, where she worked with Dr. David Ballou and Dr. Bruce Palfey on the transient-state kinetics of flavoprotein reduction. She received a M.S. in 2001 from the Université de Paris XI in Orsay, France, under the direction of Dr. Florence Lederer (CNRS, Gif-sur-Yvette). She is currently pursuing a Ph.D. in biophysics in the laboratory of Josh Wand at the University of Pennsylvania, where she uses NMR relaxation techniques to investigate the role that protein dynamics play in protein–protein interactions.

The emerging success of NMR spectroscopy in the arena of protein dynamics rests on four general areas of development over the past two decades. First and perhaps foremost, triple resonance NMR spectroscopy now provides an efficient and robust set of tools for the comprehensive resonance assignment of proteins of significant size.[10,11] These methods, in turn, derive much of their power from companion isotopic enrichment strategies,[12,13] which have been subsequently refined to allow for isotopic labeling patterns that are optimized for NMR relaxation studies (*vide infra*). Two-dimensional sampling of relaxation has allowed for comprehensive studies to be efficiently undertaken, albeit with great instrumental cost.[14−16] A variety of technical issues such as the effects of macromolecular tumbling and the influence of competing relaxation mechanisms have also been largely resolved (*vide infra*). These advances have positioned solution NMR spectroscopy to efficiently and comprehen-

Josh Wand was born and raised in Ottawa, Canada. He received his B.Sc. (honors) in biochemistry from Carleton University in Ottawa. Working under the direction of Stan Tsai, he also received a M.Sc. in bioorganic chemistry from Carleton University. He received his Ph.D. in biophysics from the University of Pennsylvania under the guidance of Walter Englander. After a short postdoctoral stint in solid-state NMR at the National Research Council of Canada with I. C. P. Smith, he joined the faculty of the Institute for Cancer Research. He subsequently spent time on the faculties of the University of Illinois at Urbana-Champaign and the State University of New York at Buffalo. He is currently the Benjamin Rush Professor of Biochemistry and chair of the graduate group in biochemistry and molecular biophysics at the University of Pennsylvania, where he continues to employ novel applications of solution NMR to questions in protein biophysics.

sively characterize the fast internal dynamics of proteins of significant size.

This review seeks to provide a compact but reasonably complete description of the theoretical and technical foundation for solution NMR relaxation methods that are currently being brought to bear on fast sub-nanosecond protein side chain dynamics and to present a summary of current findings and their possible significance. A survey of basic observations about side chain dynamics derived from NMR relaxation studies is presented along with several analyses meant to dispel commonly held but apparently inaccurate correlations between dynamics, structure, and function. How dynamics can enter into fundamental thermodynamic and kinetic aspects of protein function is also reviewed and illustrated with intriguing results from several systems that point to a promising future for this area of inquiry.

2. Theory

2.1. Formal Relationship between Fast Dynamics and Relaxation

Relaxation of nuclear spins in liquid samples is caused by fluctuating local fields, such as chemical shielding anisotropy, dipole−dipole, and quadrupolar interactions. Rapid molecular motions of large amplitude and random character impose time modulation on these local fields. The goal of this section is to summarize the mathematical framework used to obtain the information about these motions from the relaxation behavior of NMR observables; in that, the treatment of Abragam[17] and Hoffman[18] will be followed. The density matrix formalism is employed to represent the properties of the statistical ensemble of spins in a liquid sample, while the surroundings (or lattice) are treated classically. To obtain the correct behavior of the density matrix as it evolves toward its final state, this treatment has to be corrected by replacing the density matrix

operator with its deviation from the equilibrium value. If the time behavior of the density matrix is known, one is able to obtain the time behavior of any observable by taking a trace of the product between the observable and corresponding density matrix operators.

We start with the Liouville−von Neumann equation that describes time evolution of the density matrix $\rho(t)$ under the influence of a time-dependent Hamiltonian $\mathbf{H}(t)$:

$$\frac{\mathrm{d}\boldsymbol{\rho}}{\mathrm{d}t} = -i[\mathbf{H},\boldsymbol{\rho}] \tag{1a}$$

$$\mathbf{H}(t) = \mathbf{H}_0 + \mathbf{H}_{\mathrm{r}}(t) = \omega\mathbf{I}_z + \mathbf{H}_{\mathrm{r}}(t) \tag{1b}$$

The time-independent part of the Hamiltonian $\mathbf{H}_0$ represents a Zeeman interaction of the spin angular momentum $\mathbf{I}_z$ with the static magnetic field, while $\mathbf{H}_{\mathrm{r}}(t)$ is a random Hamiltonian that describes the fluctuating local fields; ω is the Larmor precession frequency. It is convenient to use an interaction representation of eq 1a:

$$\frac{\mathrm{d}\tilde{\boldsymbol{\rho}}}{\mathrm{d}t} = -i[\tilde{\mathbf{H}}_{\mathrm{r}}(t),\tilde{\boldsymbol{\rho}}] \tag{2}$$

where $\tilde{\rho} = \mathrm{e}^{i\mathbf{H}_0 t}\rho\mathrm{e}^{-i\mathbf{H}_0 t}$ and $\tilde{\mathbf{H}}_{\mathrm{r}}(t) = \mathrm{e}^{i\mathbf{H}_0 t}\mathbf{H}_{\mathrm{r}}(t)\mathrm{e}^{-i\mathbf{H}_0 t}$. The bar in eq 2 indicates the average over the entire spin ensemble. Equation 2 can be successively integrated to second order and differentiated to become

$$\frac{\mathrm{d}\tilde{\boldsymbol{\rho}}}{\mathrm{d}t} = -i\overline{[\tilde{\mathbf{H}}_{\mathrm{r}}(t),\tilde{\boldsymbol{\rho}}(0)]} - \int_0^t \overline{[\tilde{\mathbf{H}}_{\mathrm{r}}(t),[\tilde{\mathbf{H}}_{\mathrm{r}}(t-\tau),\tilde{\boldsymbol{\rho}}(0)]]}\,\mathrm{d}\tau \tag{3}$$

Equation 3 can be simplified using the following assumptions:

(i) In the first term, the random Hamiltonian and the density matrix operator are uncorrelated and can be averaged separately over the spin ensemble. The ensemble average of $\tilde{\mathbf{H}}_{\mathrm{r}}(t)$ is zero, which eliminates the first term from the equation.

(ii) $\tilde{\rho}(0)$ can be validly replaced with $\tilde{\rho}(t)$.

(iii) The upper limit of the integral can be extended to infinity.

An excellent discussion of the validity of these assumptions is given by Abragam.[17] The simplified equation for the density matrix evolution in the interaction frame is given by

$$\frac{\mathrm{d}\tilde{\boldsymbol{\rho}}}{\mathrm{d}t} = -\int_0^\infty \overline{[\tilde{\mathbf{H}}_{\mathrm{r}}(t),[\tilde{\mathbf{H}}_{\mathrm{r}}(t-\tau),\tilde{\boldsymbol{\rho}}(t)]]}\,\mathrm{d}\tau \tag{4}$$

Since our ultimate goal is to obtain the time behavior of NMR observables, it is convenient to cast eq 4 in operator form. Although this increases the dimensionality of the problem, it makes the calculation physically intuitive and allows one to exploit useful commutation relationships between the spin operators. The density matrix operator can be expanded as a linear combination of the basis operators $\mathbf{Q}_k$ with time-dependent coefficients $\rho_k(t)$:

$$\tilde{\boldsymbol{\rho}}(t) = \sum_k \rho_k(t)\mathbf{Q}_k^\dagger \tag{5}$$

where the basis operators satisfy the orthonormality condition: $\mathrm{Tr}\{\mathbf{Q}_k^\dagger\mathbf{Q}_l\} = \delta_{kl}$. Substituting eq 5 into eq 4 and making use of the identity $\mathrm{Tr}\{\mathbf{A}[\mathbf{B},[\mathbf{C},\mathbf{D}]]\} =$

$-\mathrm{Tr}\{[\mathbf{A},\mathbf{B}][\mathbf{D},\mathbf{C}]\}$, we obtain the expression for the time evolution of $\rho_i(t)$ and the relaxation matrix element Γ_{ik}:

$$\frac{\mathrm{d}\rho_i(t)}{\mathrm{d}t} = \sum_k \Gamma_{ik}\rho_k(t) \tag{6a}$$

$$\Gamma_{ik} = \frac{1}{2}\int_{-\infty}^{+\infty}\overline{\mathrm{Tr}\{[\mathbf{Q}_i,\tilde{\mathbf{H}}_{\mathrm{r}}(t)][\mathbf{Q}_k^\dagger,\tilde{\mathbf{H}}_{\mathrm{r}}(t-\tau)]\}}\,\mathrm{d}\tau \tag{6b}$$

In turn, the random Hamiltonian can be written as a sum of scalar products of irreducible spherical tensors:

$$\mathbf{H}_{\mathrm{r}}(t) = C^\lambda\sum_\lambda\sum_{l,m}(-1)^m\mathbf{T}_{l,m}^\lambda\,F_{l,-m}^\lambda(t) \tag{7}$$

C^λ is the interaction constant; $\mathbf{T}_{l,m}^\lambda$ are the spin operators in irreducible tensor form, corresponding to an interaction λ and having a rank l and a component index m; and $F_{l,-m}^\lambda(t)$ are the spatial random functions proportional to the spherical harmonics. $\mathbf{T}_{l,m}^\lambda$ and $F_{l,m}^\lambda$ have the following useful properties:

$$[\mathbf{I}_z,\mathbf{T}_{l,m}^\lambda] = m\mathbf{T}_{l,m}^\lambda \text{ and hence } \mathrm{e}^{i\mathbf{H}_0 t}\mathbf{T}_{l,m}^\lambda\mathrm{e}^{-i\mathbf{H}_0 t} = \mathrm{e}^{im\omega t}\mathbf{T}_{l,m}^\lambda \tag{8a}$$

$$\mathbf{T}_{l,-m}^\lambda = (-1)^m(\mathbf{T}_{l,m}^\lambda)^\dagger \tag{8b}$$

$$F_{l,-m}^\lambda = (-1)^m(F_{l,m}^\lambda)^* \tag{8c}$$

Transforming the random Hamiltonian into the interaction frame

$$\tilde{\mathbf{H}}_{\mathrm{r}}(t) = C^\lambda\sum_\lambda\sum_{l,m}(-1)^m\mathrm{e}^{i\omega m t}\mathbf{T}_{l,m}^\lambda F_{l,-m}^\lambda(t) \tag{9}$$

and substituting this expression into the equation for Γ_{ik} (see eq 6b) gives

$$\Gamma_{ik} = \frac{1}{2}C^{\lambda'}C^{\lambda''}\sum_{\lambda'}\sum_{\lambda''}\sum_{l',m'}\sum_{l'',m''}(-1)^{m'+m''}\mathrm{e}^{i\omega(m'+m'')t} \times$$

$$\mathrm{Tr}\{[\mathbf{Q}_i,\mathbf{T}_{l',m'}^{\lambda'}][\mathbf{Q}_k^\dagger,\mathbf{T}_{l'',m''}^{\lambda''}]\} \times$$

$$\int_{-\infty}^{+\infty}\overline{F_{l',-m'}^{\lambda'}(t)\,F_{l'',-m''}^{\lambda''}(t-\tau)}\mathrm{e}^{-i\omega m''\tau}\,\mathrm{d}\tau \tag{10}$$

After some rearrangement, the integral in eq 10 can be identified as the spectral density function $J_{l'l''m'm''}^{\lambda'\lambda''}(\omega)$:

$$J_{l'l''m'm''}^{\lambda'\lambda''}(\omega) = \int_{-\infty}^{+\infty}\overline{(F_{l',m'}^{\lambda'}(t))^*\,F_{l'',-m''}^{\lambda''}(t+\tau)}\mathrm{e}^{-i\omega m''\tau}\,\mathrm{d}\tau \tag{11}$$

Spectral density and correlation functions will be discussed in more detail in section 4 of this review. For now, it suffices to say that the spectral density functions represent the frequency spectra of molecular motions.

Since the lattice is assumed to be in thermal equilibrium, the spectral density functions do not depend on time t. The only time dependence is imposed on Γ_{ik} by the exponential term $\mathrm{e}^{i\omega(m'+m'')t}$. This term oscillates with Larmor frequency ω, which is large compared to the characteristic frequencies of Γ_{ik}. Therefore, the terms with $m' + m'' \neq 0$ contribute negligibly to Γ_{ik} and can be neglected. In an isotropic medium, the spectral density given by eq 11 vanishes unless

the ranks of the correlated interactions are equal, i.e., $l' = l''$.[18] As a result, eq 10 can be rewritten in the following form:

$$\Gamma_{ik} = \frac{1}{2}C^{\lambda'}C^{\lambda''}\sum_{\lambda',\lambda''}\sum_{l,m}(-1)^m \times$$
$$\text{Tr}\{[\mathbf{Q}_i,\mathbf{T}_{l,m}^{\lambda'}][\mathbf{Q}_k^\dagger,\mathbf{T}_{l,-m}^{\lambda''}]\}J_{lm}^{\lambda'\lambda''}(m\omega) \quad (12a)$$

$$J_{lm}^{\lambda'\lambda''}(m\omega) = \int_{-\infty}^{+\infty}\overline{(F_{l',m}^{\lambda'}(t))^* F_{l'',m}^{\lambda''}(t+\tau)}e^{-i\omega m\tau}\,d\tau \quad (12b)$$

Relaxation matrix elements with $\lambda' = \lambda''$ and $\lambda' \neq \lambda''$ are referred to as the autocorrelated and cross-correlated relaxation rates, respectively. It is evident from eq 12a that the elements of relaxation matrix Γ_{ik} are linear combinations of the spectral density functions sampled at certain frequencies, with coefficients provided by the trace taken over the product of commutators. Using eqs 12, we can now calculate Γ_{ik} for specific spin systems found in protein side chains. The corresponding relaxation times T_{ik} are the inverses of the matrix elements Γ_{ik}:

$$T_{ik} = -1/\Gamma_{ik} \quad (13)$$

Below, we derive autorelaxation rates for the local fields responsible for the relaxation in isotopically enriched protein side chains: heteronuclear dipole–dipole interaction, chemical shielding anisotropy (CSA), and electrostatic coupling between the nuclear quadrupole moment and the electric field gradient. In addition, cross-correlated relaxation (or relaxation interference) between two dipole–dipole interactions is considered.

2.2. Heteronuclear Dipole–Dipole Interactions

We consider an isolated system of two spins $\frac{1}{2}$, I and S, that belong to different nuclear species. The time-dependent Hamiltonian for this system is

$$\mathbf{H}(t) = \mathbf{H}_0 + \mathbf{H}_{DD}(t) \quad (14a)$$

$$\mathbf{H}_0 = \omega_I\mathbf{I}_z + \omega_S\mathbf{S}_z \quad (14b)$$

where ω_I and ω_S are the Larmor precession frequencies of spins I and S, and $\mathbf{H}_{DD}(t)$ is the heteronuclear dipolar coupling Hamiltonian in the laboratory frame:

$$\mathbf{H}_{DD}(t) = d\sum_m(-1)^m\mathbf{T}_{2,m}F_{2,-m}(t) \quad (15)$$

The dipolar coupling constant d is defined as follows: $d = -\mu_0\gamma_I\gamma_S\hbar/4\pi r_{IS}^3$, where μ_0 is the magnetic permeability, $\gamma_{I(S)}$ is the gyromagnetic ratio of the $I(S)$ spin, $\hbar$ is Planck's constant divided by 2π, and r_{IS} is the distance between nuclei I and S, which for the moment we assume to be fixed. A set of spherical tensor operators $\mathbf{T}_{l,m}$ with rank $l = 1, 2$ is given below:

$$\mathbf{T}_{1,0} = \mathbf{S}_z$$

$$\mathbf{T}_{1,1} = -\frac{1}{\sqrt{2}}\mathbf{S}_+ = -\mathbf{T}_{1,-1}^\dagger$$

$$\mathbf{T}_{2,0} = 2\mathbf{I}_z\mathbf{S}_z - \frac{1}{2}(\mathbf{I}_+\mathbf{S}_- + \mathbf{I}_-\mathbf{S}_+) = 3\mathbf{I}_z\mathbf{S}_z - \mathbf{IS}$$

$$\mathbf{T}_{2,1} = -\sqrt{\frac{3}{2}}(\mathbf{I}_+\mathbf{S}_z + \mathbf{I}_z\mathbf{S}_+) = -\mathbf{T}_{2,-1}^\dagger$$

$$\mathbf{T}_{2,2} = \sqrt{\frac{3}{2}}\mathbf{I}_+\mathbf{S}_+ = \mathbf{T}_{2,-2}^\dagger \quad (16)$$

Our goal is to derive the expression for T_1, the spin–lattice relaxation time, of nucleus S, using eq 12a. We start with the dipolar Hamiltonian $\mathbf{H}_{DD}(t)$ and calculate its transformation to the double interaction frame defined as $\mathbf{U} = e^{i(\omega_I\mathbf{I}_z+\omega_S\mathbf{S}_z)t}$. To make full use of the property of eq 8a, it is convenient to represent spherical tensors of rank 2 as a sum of the products of spherical tensors of rank 1:

$$\tilde{\mathbf{T}}_{2,0} = \mathbf{U}(2\mathbf{T}_{1,0}(I)\,\mathbf{T}_{1,0}(S) + \mathbf{T}_{1,1}(I)\,\mathbf{T}_{1,-1}(S) + $$
$$\mathbf{T}_{1,-1}(I)\,\mathbf{T}_{1,1}(S))\mathbf{U}^{-1}$$

$$= 2\mathbf{I}_z\mathbf{S}_z - \frac{1}{2}\mathbf{I}_+\mathbf{S}_-e^{i(\omega_I-\omega_S)t} - \frac{1}{2}\mathbf{I}_-\mathbf{S}_+e^{-i(\omega_I-\omega_S)t}$$

$$\tilde{\mathbf{T}}_{2,1} = -\sqrt{\frac{3}{2}}\mathbf{I}_+\mathbf{S}_ze^{i\omega_It} - \sqrt{\frac{3}{2}}\mathbf{I}_z\mathbf{S}_+e^{i\omega_St} = -\tilde{\mathbf{T}}_{2,-1}^\dagger$$

$$\tilde{\mathbf{T}}_{2,2} = \sqrt{\frac{3}{2}}\mathbf{I}_+\mathbf{S}_+e^{i(\omega_I+\omega_S)t} = \tilde{\mathbf{T}}_{2,-2}^\dagger \quad (17)$$

To calculate T_1, we select $\mathbf{S}_z$ as the basis operator, which is normalized in the product basis of the $I-S$ spin system having the following set of four states: $|\frac{1}{2},\frac{1}{2}\rangle$, $|\frac{1}{2},-\frac{1}{2}\rangle$, $|-\frac{1}{2},\frac{1}{2}\rangle$, and $|-\frac{1}{2},-\frac{1}{2}\rangle$. The transformed spherical tensors of eqs 17 can now be substituted directly into eq 12a, with characteristic frequencies of the spectral density functions given by the exponents in eqs 17. Since $\mathbf{S}_z$ commutes with the $2\mathbf{I}_z\mathbf{S}_z$ operator of $\tilde{\mathbf{T}}_{2,0}$ and the $\mathbf{I}_+\mathbf{S}_z$ operator of $\tilde{\mathbf{T}}_{2,1}$, the contributions of $J_0(0)$ and $J_1(\omega_I)$ into the spin–lattice relaxation rate of spin S vanish. Note that since we consider an autorelaxation process brought about by a spin interaction of rank 2, the indices l', l'', λ', λ'' can be dropped from the spectral density function notation given in eq 11. The tensor components with $m = 0$ give rise to the only spectral density term, $J_0(\omega_I - \omega_S)$, with the coefficient given by the following double commutator:

$J_0(\omega_I - \omega_S)$:
$$\text{Tr}\{[\mathbf{S}_z,-\tfrac{1}{2}\mathbf{I}_+\mathbf{S}_-][\mathbf{S}_z,-\tfrac{1}{2}\mathbf{I}_-\mathbf{S}_+]\} = $$
$$-\tfrac{1}{4}\text{Tr}\{\mathbf{I}_+\mathbf{S}_-(\mathbf{I}_-\mathbf{S}_+)\} = -\tfrac{1}{4}$$

$$\text{Tr}\{[\mathbf{S}_z,-\tfrac{1}{2}\mathbf{I}_-\mathbf{S}_+][\mathbf{S}_z,-\tfrac{1}{2}\mathbf{I}_+\mathbf{S}_-]\} = -\tfrac{1}{4} \quad (18)$$

Similarly, for $m = \pm1$ tensor components, there is only one spectral density term, $J_1(\omega_S)$:

$J_1(\omega_S)$:

$$\mathrm{Tr}\{[\mathbf{S}_z,-\sqrt{^3/_2}\mathbf{I}_z\mathbf{S}_+][\mathbf{S}_z,\sqrt{^3/_2}\mathbf{I}_z\mathbf{S}_-]\} =$$
$$^3/_2\mathrm{Tr}\{\mathbf{I}_z\mathbf{S}_+(\mathbf{I}_z\mathbf{S}_-)\} = {}^3/_4$$

$$\mathrm{Tr}\{[\mathbf{S}_z,\sqrt{^3/_2}\mathbf{I}_z\mathbf{S}_-][\mathbf{S}_z,-\sqrt{^3/_2}\mathbf{I}_z\mathbf{S}_+]\} = {}^3/_4 \quad (19)$$

Finally, for $m = \pm 2$ and $J_2(\omega_I + \omega_S)$, we obtain

$J_2(\omega_I + \omega_S)$:

$$\mathrm{Tr}\{[\mathbf{S}_z,\sqrt{^3/_2}\mathbf{I}_+\mathbf{S}_+][\mathbf{S}_z,\sqrt{^3/_2}\mathbf{I}_-\mathbf{S}_-]\} =$$
$$- {}^3/_2\mathrm{Tr}\{\mathbf{I}_+\mathbf{S}_+(\mathbf{I}_-\mathbf{S}_-)\} = - {}^3/_2$$

$$\mathrm{Tr}\{[\mathbf{S}_z,\sqrt{^3/_2}\mathbf{I}_-\mathbf{S}_-][\mathbf{S}_z,\sqrt{^3/_2}\mathbf{I}_+\mathbf{S}_+]\} = - {}^3/_2 \quad (20)$$

Collecting the terms of eqs 18−20, we arrive at the final expressions for the autorelaxation matrix element $\Gamma^{DD}_{S_z,S_z}$ and spin−lattice relaxation time $T_1^{DD}(S)$:

$$\frac{1}{T_1^{DD}(S)} = -\Gamma^{DD}_{S_z,S_z} =$$
$$\frac{1}{4}d^2[J_0(\omega_I - \omega_S) + 3J_1(\omega_S) + 6J_2(\omega_I + \omega_S)] \quad (21)$$

Other relaxation parameters, such as T_2 (basis operator $(1/\sqrt{2})\mathbf{S}_+$) and cross-relaxation rate σ (basis operators $\mathbf{I}_z$ and $\mathbf{S}_z$) can be similarly derived using eq 12a:

$$\frac{1}{T_2^{DD}(S)} = -\Gamma^{DD}_{1/(\sqrt{2})\mathbf{S}_+,1/(\sqrt{2})\mathbf{S}_+} = \frac{1}{8}d^2[4J_0(0) +$$
$$J_0(\omega_I - \omega_S) + 6J_1(\omega_I) + 3J_1(\omega_S) + 6J_2(\omega_I + \omega_S)] \quad (22a)$$

$$\sigma = -\Gamma^{DD}_{I_z,S_z} = \frac{1}{4}d^2[6J_2(\omega_I + \omega_S) - J_0(\omega_I - \omega_S)] \quad (22b)$$

The corresponding derivations can be found in numerous textbooks and reviews.[17,19−21]

2.3. Chemical Shielding Anisotropy

In this section, we consider a contribution of the chemical shielding anisotropy (CSA) to the spin−lattice relaxation time of spin S for a simplified case of the axially symmetric CSA tensor. The time-dependent part of the CSA Hamiltonian in the laboratory frame can be written exactly as in eq 15, with the operator $\mathbf{I}$ replaced by the magnetic field vector $\mathbf{B}_0$ in the expression for the spherical tensors:

$$\mathbf{H}_{CSA}(t) = C^{CSA}\sum_m(-1)^m\mathbf{T}_{2,m}F_{2,-m}(t) \quad (23)$$

The interaction constant C^{CSA} is defined as $C^{CSA} = \gamma_S(\sigma_\| - \sigma_\perp)/3$, where $\sigma_\|$ and $\sigma_\perp$ are the principal values of the CSA tensor along the z_{PAS} and $x_{PAS}(y_{PAS})$ axes of its principal axis system (PAS). Equation 23 can be simplified by realizing that, in the laboratory frame, the vector of the static magnetic field is oriented along the z_{LAB} axis, i.e., $\mathbf{B}_0 = B_0\hat{\mathbf{z}}_{LAB}$. The expression for the Hamiltonian then becomes

$$\mathbf{H}_{CSA}(t) =$$
$$C^{CSA}B_0[2\mathbf{S}_zF_{2,0}(t) + \sqrt{^3/_2}\mathbf{S}_+F_{2,-1}(t) - \sqrt{^3/_2}\mathbf{S}_-F_{2,1}(t)] \quad (24)$$

We select $(\sqrt{2})\mathbf{S}_z$ as the basis operator normalized in the $|^1/_2\rangle, |-^1/_2\rangle$ basis. It is clear from eq 24 that only two spectral density terms, $J_0(0)$ and $J_1(\omega_S)$, contribute to the relaxation matrix elements. Of the two, the $J_0(0)$ term vanishes since $\mathbf{S}_z$ commutes with itself. The coefficients for the $J_1(\omega_S)$ term are given by the following traces taken over double commutators:

$$J_1(\omega_S): \quad 2\frac{3}{2}\mathrm{Tr}\{[\mathbf{S}_z,\mathbf{S}_+][\mathbf{S}_z,-\mathbf{S}_-]\} = 3\mathrm{Tr}\{\mathbf{S}_+\mathbf{S}_-\} = 3$$

$$2\frac{3}{2}\mathrm{Tr}\{[\mathbf{S}_z,\mathbf{S}_-][\mathbf{S}_z,-\mathbf{S}_+]\} = 3\mathrm{Tr}\{\mathbf{S}_-\mathbf{S}_+\} = 3 \quad (25)$$

The final expression for the relaxation matrix elements $\Gamma^{CSA}_{(\sqrt{2})S_z,(\sqrt{2})S_z}$ and the corresponding spin−lattice relaxation time $T_1^{CSA}(S)$ is

$$\frac{1}{T_1^{CSA}(S)} = -\Gamma^{CSA}_{(\sqrt{2})S_z,(\sqrt{2})S_z} = c^2J_1(\omega_S) \quad (26)$$

where $c = \gamma_SB_0(\sigma_\| - \sigma_\perp)/\sqrt{3}$. The expression for $T_2^{CSA}(S)$ can similarly be derived:

$$\frac{1}{T_2^{CSA}(S)} = -\Gamma^{CSA}_{S_+,S_+} = \frac{1}{6}c^2[4J_0(0) + 3J_1(\omega_S)] \quad (27)$$

In contrast to the case of the dipole−dipole interactions, the CSA interaction constant depends on the strength of the static magnetic field B_0. As a consequence, the contribution of the CSA to the relaxation rates increases with the increase of the static magnetic field strength.

2.4. Quadrupolar Interaction

Quadrupolar interaction is the electrostatic interaction between the quadrupolar moment of a nucleus having a spin ≥ 1 and the electric field gradient. In this section, we consider the quadrupolar interaction of the isolated ^{2}H nucleus. The quadrupolar interaction constant for ^{2}H exceeds the strength of other local fields, such as dipole−dipole interactions and CSA, by approximately 1 to 2 orders of magnitude, thereby making the quadrupolar interaction a dominating relaxation mechanism in fractionally deuterated protein side chains. Similar to the dipole−dipole interaction and CSA Hamiltonians, the quadrupolar Hamiltonian is a second-rank tensor and can be written in the laboratory frame as

$$\mathbf{H}_Q(t) = C^Q\sum_m(-1)^m\mathbf{T}_{2,m}F_{2,-m}(t) \quad (28)$$

The interaction constant C^Q is defined as $C^Q = e^2qQ/4\hbar I(2I - 1) = e^2qQ/4\hbar$, where e is the elementary electronic charge, Q is a nuclear quadrupole moment, q is the principal value of the electric gradient tensor, and I is the spin of the nucleus, equal to 1 for ^{2}H. A full description of spin 1 in the operator space requires $3^2 = 9$ operators that can be conveniently chosen as normalized spherical harmonics given by eq 17, with spin operator $\mathbf{S}$ replaced by $\mathbf{I}$. The full

relaxation matrix for spin 1 having five independent elements was calculated by Jacobsen and co-workers.[22] In this section, we present a derivation of T_1, the spin–lattice relaxation time for ^{2}H. The rest of the relaxation parameters can be derived using similar procedures.

We select $(1/\sqrt{2})\mathbf{I}_z$ as the basis operator, normalized in the following basis: $|1,-1\rangle$, $|1,0\rangle$, $|1,1\rangle$, and we rewrite the spherical tensors of eq 17 in terms of the single spin operator $\mathbf{I}$. Since $\mathbf{I}_z$ commutes with $\mathbf{T}_{2,0}$, $J_0(0)$ does not contribute to the spin–lattice relaxation time of ^{2}H. The terms with $m = \pm 1$ and $m = \pm 2$ give rise to the following spectral density coefficients:

$$J(\omega_D): \quad \frac{1}{2}\mathrm{Tr}\{[\mathbf{I}_z,\mathbf{T}_{2,1}][\mathbf{I}_z,\mathbf{T}_{2,-1}]\} = -\frac{1}{2}\mathrm{Tr}\{\mathbf{T}_{2,1}\mathbf{T}_{2,-1}\} =$$
$$\frac{3}{4}\mathrm{Tr}\{(\mathbf{I}_+\mathbf{I}_z + \mathbf{I}_+\mathbf{I}_z)(\mathbf{I}_-\mathbf{I}_z + \mathbf{I}_-\mathbf{I}_z)\} = 3$$

$$\frac{1}{2}\mathrm{Tr}\{[\mathbf{I}_z,\mathbf{T}_{2,-1}][\mathbf{I}_z,\mathbf{T}_{2,1}]\} = 3 \tag{29a}$$

$$J(2\omega_D): \quad \frac{1}{2}\mathrm{Tr}\{[\mathbf{I}_z,\mathbf{T}_{2,2}][\mathbf{I}_z,\mathbf{T}_{2,-2}]\} = -2\mathrm{Tr}\{\mathbf{T}_{2,2}\mathbf{T}_{2,-2}\} =$$
$$-3\mathrm{Tr}\{(\mathbf{I}_+\mathbf{I}_+)(\mathbf{I}_-\mathbf{I}_-)\} = -12$$

$$\frac{1}{2}\mathrm{Tr}\{[\mathbf{I}_z,\mathbf{T}_{2,-2}][\mathbf{I}_z,\mathbf{T}_{2,2}]\} = -12 \tag{29b}$$

Collecting the terms of eqs 29, we arrive at the expressions for the relaxation matrix element $\Gamma^Q_{(1/2)I_z,(1/2)I_z}$ and the corresponding relaxation time $T_1{}^Q$:

$$\frac{1}{T_1{}^Q} = -\Gamma^Q_{(1/2)I_z,(1/2)I_z} = 3(C^Q)^2[J(\omega_D) + 4J(2\omega_D)] \tag{30}$$

The expressions for other relaxation parameters can be found in ref 22 and are

$$\frac{1}{T_2{}^Q} = -\Gamma^Q_{(1/2)I_+,(1/2)I_+} = 3(C^Q)^2\left[\frac{3}{2}J(0) + \frac{5}{2}J(\omega_D) + J(2\omega_D)\right]$$

$$\frac{1}{T_{QO}{}^Q} = -\Gamma^Q_{(1/\sqrt{6})(3I_z^2-I^2),(1/\sqrt{6})(3I_z^2-I^2)} = 3(C^Q)^2[3J(\omega_D)]$$

$$\frac{1}{T_{DQ}{}^Q} = -\Gamma^Q_{(1/2)I_+I_+,(1/2)I_+I_+} = 3(C^Q)^2[J(\omega_D) + 2J(2\omega_D)]$$

$$\frac{1}{T_{SQAF}{}^Q} = -\Gamma^Q_{1/2(I_zI_+ + I_zI_+),1/2(I_zI_+ + I_zI_+)} =$$
$$3(C^Q)^2\left[\frac{3}{2}J(0) + \frac{1}{2}J(\omega_D) + J(2\omega_D)\right] \tag{31}$$

where the subscripts QO, DQ, and SQAF stand for the quadrupolar order, double-quantum, and single-quantum antiphase coherences. The five relaxation rates given by eqs 30 and 31 can be measured independently using the NMR methodology developed by Kay and co-workers.[23,24] These rates form an overdetermined and self-consistent data set, which can be used to extract information about motions of protein side chains.

2.5. Cross-Correlated Relaxation or Relaxation Interference

So far we have considered autorelaxation mechanisms brought about by one type of NMR local field. The interference between two different relaxation mechanisms, or cross-correlated relaxation, has found applications in the investigation of side chain dynamics.[25–27] Formally, cross-correlated relaxation rates can be described by the relaxation matrix elements of eq 12a with $\lambda' \neq \lambda''$. The interference can occur between, e.g., two different dipole–dipole interactions, between two CSA interactions, and between the CSA and dipole–dipole interactions. One of the experimental manifestations of the cross-correlated relaxation is the different relaxation behavior of the NMR lines in J-coupled spin multiplets.

We consider dipole–dipole cross-correlated relaxation in a system of 3 spins $^1/_2$, I_1–S–I_2. An example of such a spin system is a methylene group of a protein side chain, with two ^{1}H magnetic dipoles sharing a common ^{13}C spin. Since the J-coupling constants of I_1–S and I_2–S are almost identical, in the absence of heteronuclear decoupling, the S nucleus gives rise to a triplet. The outer components of the triplet have unequal line widths (or intensities) due to the dipole–dipole cross-correlated relaxation.

To calculate the contribution of the I–S dipole–dipole cross-correlations to the longitudinal relaxation of spin S, it is convenient to choose the basis operators that correspond to one- and three-spin orders, $(1/\sqrt{2})\mathbf{S}_z$ and $(\sqrt{8})\mathbf{S}_z\mathbf{I}_{1z}\mathbf{I}_{2z}$; the operators are normalized in the product basis containing all eight combinations of the "up" and "down" states for every spin. The next step is to select the spherical tensors with matching frequencies (see eqs 17). Provided that spins I_1 and I_2 have nondegenerate chemical shifts, the two tensor components that remain are $2\mathbf{I}_{1z(2z)}\mathbf{S}_z$ of $\tilde{\mathbf{T}}_{2,0}$ and $\mp(\sqrt{3}/2)\mathbf{I}_{1z(2z)}\mathbf{S}_\pm$ of $\tilde{\mathbf{T}}_{2,\pm1}$, giving rise to the $J_0^{DD1,DD2}(0)$ and $J_1^{DD1,DD2}(\omega_S)$ spectral density terms. The $J_0^{DD1,DD2}(0)$ term vanishes since $\mathbf{S}_z$ commutes with $\tilde{\mathbf{T}}_{2,0}$, while the contribution of $J_1^{DD1,DD2}(\omega_S)$ can be calculated using standard procedures:

$$J_1^{DD1,DD2}(\omega_S):$$
$$2\mathrm{Tr}\{[\mathbf{S}_z,\mathbf{T}_{2,1}^{DD1}][\mathbf{S}_z\mathbf{I}_{1z}\mathbf{I}_{2z},\mathbf{T}_{2,-1}^{DD2}]\} =$$
$$-3\mathrm{Tr}\{[\mathbf{S}_z\mathbf{I}_{1z}\mathbf{S}_+][\mathbf{S}_z\mathbf{I}_{1z}\mathbf{I}_{2z},\mathbf{I}_{2z}\mathbf{S}_-]\} =$$
$$3\mathrm{Tr}\{(\mathbf{S}_+\mathbf{I}_{1z}\mathbf{I}_{2z})(\mathbf{S}_-\mathbf{I}_{1z}\mathbf{I}_{2z})\} = \frac{3}{4}$$

$$2\mathrm{Tr}\{[\mathbf{S}_z,\mathbf{T}_{2,-1}^{DD1}][\mathbf{S}_z\mathbf{I}_{1z}\mathbf{I}_{2z},\mathbf{T}_{2,1}^{DD2}]\} = \frac{3}{4} \tag{32}$$

A symmetric pair of interactions between $\mathbf{T}_{2,\pm1}^{DD2}$ and $\mathbf{T}_{2,\pm1}^{DD1}$ also contributes to the cross-correlated relaxation rate, giving a factor of 2 in the final equation for $\Gamma^{DD1,DD2}_{S_z,2S_zI_{1z}I_{2z}}$. Using eq 12a, we obtain the following expression for $\Gamma^{DD1,DD2}_{S_z,2S_zI_{1z}I_{2z}}$:

$$\Gamma^{DD1,DD2}_{S_z,2S_zI_{1z}I_{2z}} = -2 \times \frac{1}{8}d^2[6J_1^{DD1,DD2}(\omega_S)] \tag{33}$$

where d is defined in eq 15.

To calculate the contribution of the I–S dipole–dipole cross-correlations to the transverse relaxation of spin S, we select $(1/2)\mathbf{S}_+$ and $2\mathbf{S}_+\mathbf{I}_{1z}\mathbf{I}_{2z}$ as basis operators. The coefficients of $J_0^{DD1,DD2}(0)$ and $J_1^{DD1,DD2}(\omega_S)$ are obtained as follows:

$J_0^{DD1,DD2}(0): \quad \mathrm{Tr}\{[\mathbf{S}_+,\mathbf{I}_{2z}\mathbf{S}_z][\mathbf{I}_{1z}\mathbf{I}_{2z}\mathbf{S}_-,2\mathbf{I}_{2z}\mathbf{S}_z]\} =$
$$-4\mathrm{Tr}\{(\mathbf{S}_+\mathbf{I}_{1z}\mathbf{I}_{2z})(\mathbf{S}_-\mathbf{I}_{1z}\mathbf{I}_{2z})\} = -1$$

$J_1^{DD1,DD2}(\omega_S): \quad \mathrm{Tr}\{[\mathbf{S}_+,\mathbf{I}_{1z}\mathbf{S}_-][\mathbf{I}_{1z}\mathbf{I}_{2z}\mathbf{S}_-,2\mathbf{I}_{2z}\mathbf{S}_+]\} =$
$$6\mathrm{Tr}\{(\mathbf{S}_z\mathbf{I}_{1z}\mathbf{I}_{2z})(\mathbf{S}_z\mathbf{I}_{1z}\mathbf{I}_{2z})\} = \frac{3}{4} \quad (34)$$

Substitution of eqs 15 and 16 into eq 12a results in the expression for $\Gamma_{S_+,S_+I_{1z}I_{2z}}^{DD1,DD2}$:

$$\Gamma_{S_+,S_+I_{1z}I_{2z}}^{DD1,DD2} = -2 \times \frac{1}{8}d^2[4J_0^{DD1,DD2}(0) + 3J_1^{DD1,DD2}(\omega_S)] \quad (35)$$

The cross-correlation spectral density functions, $J_m^{DD1,DD2}(\omega)$, can be further simplified for the case of isotropic molecular tumbling.[28,29]

In summary, we presented derivations of autocorrelated and cross-correlated relaxation rates for several relaxation mechanisms. These rates are linear combinations of autocorrelated and cross-correlated spectral density functions sampled at characteristic frequencies and are proportional to the square of the appropriate interaction constants. In the next section, we review experimental approaches used for the selection and quantification of these relaxation pathways. Interpretation of relaxation parameters in terms of different motion models is the subject of section 4.

3. Experimental Development

3.1. Purity of the Relaxation Mechanism

A meaningful interpretation of NMR relaxation data relies on the precise knowledge of relaxation mechanisms in a given spin system. Protein side chains mostly include methyl (AX$_3$ spin system), methylene (AMX or AX$_2$), methine (AX), and aromatic groups linked by covalent bonds. If all nuclei of a protein side chain were magnetically active, a correct interpretation of the relaxation behavior would require knowledge of the exact geometry and magnitude of all tensorial interactions contributing to a great many relaxation pathways, making the data analysis cumbersome. Hence, recent developments in solution NMR relaxation techniques aim at achieving purity and simplicity of relaxation mechanisms by combining isotope labeling schemes with NMR pulse sequence development. Along with multi-spin relaxation, spectral resolution is an important issue to consider when implementing relaxation experiments. NMR relaxation pulse sequences are usually based on two-dimensional HSQC experiments that correlate the chemical shifts of two nuclei, with variable time delays inserted to record relaxation of the appropriate spin coherences. In both ^{13}C- and ^{2}H-based autorelaxation experiments, the site resolution is achieved by collecting ^{13}C$-^1$H chemical shift correlation spectra. NMR resonances of methyl groups tend to be well-resolved due to rotational averaging of the ^{13}C$-^1$H interactions and have high signal-to-noise ratios due to the fact that three methyl protons contribute to the same signal. Nevertheless, it is difficult to obtain a complete sampling of methyl dynamics in large molecular weight proteins. The situation is even worse for methylene groups, where the ^{13}C$-^1$H spectral region has a usable spectral resolution generally only in proteins of less than 100 amino acids.[25] The problem of spectral resolution can be partially alleviated by using suitable isotope labeling schemes, described in detail below, and a

3D acquisition mode, as implemented in the cross-correlated relaxation experiments. In addition to the relaxation mechanisms described in part 2, scalar couplings between nuclei, although being an order of magnitude smaller than dipole−dipole interactions, significantly complicate faithful observation of relaxation phenomena. Below, we consider isotope labeling schemes and pulse sequences designed to alleviate the problems of multi-spin relaxation, J-coupling interactions, and spectral resolution.

3.2. Isotope Labeling Schemes

Optimization of relaxation studies rests significantly on attaining a well-understood relaxation mechanism and site resolution. Both require specialized isotopic enrichment. A comprehensive review of isotope labeling schemes used for protein solution NMR spectroscopy can be found elsewhere.[30,31] Here, we will focus on the isotope labeling schemes specifically designed for the measurements of protein side chain dynamics. These labeling schemes are summarized in Table 1.

A major complication encountered in the relaxation studies of uniformly ^{13}C-enriched proteins is the contribution of ^{13}C$-$ ^{13}C interactions to the observed relaxation behavior, which becomes multiexponential. In early ^{13}C relaxation experiments, this problem was overcome by supplementing the growth medium with specifically labeled amino acids[32,33] or using natural abundance ^{13}C spectroscopy.[34] Later, a uniform sampling of the dynamics of protein sites became possible with the development of the fractional ^{13}C labeling scheme that made use of a mixture of labeled and unlabeled acetates (see Table 1).[15,35] When this mixture of acetates is used as the sole carbon source, carbon sites with one bonded carbon have a 15% probability of being bonded to a ^{13}C nucleus and sites with two bonded carbons have a 30% probability of being bonded to at least one ^{13}C nucleus. The contributions of ^{13}C$-^{13}$C pairs to the final signal can be suppressed using the low-pass ^{13}C filter developed by Wand et al.[15] This pulse sequence makes use of the fact that the amplitudes of the signals originating from ^{13}C$-^{13}$C pairs are modulated by a $^1J_{CC}$-dependent cosine function and, thus, can be forced to zero by a judicious choice of the constant-time delay.

A marked improvement in the sensitivity of ^{13}C-based relaxation experiments was achieved by using 3-^{13}C-labeled pyruvate as the sole carbon source.[36] Originally used for the incorporation of methyl protons in perdeuterated proteins,[37] pyruvate preferentially labels Ala$^\beta$, Ile$^\gamma$, Val$^\gamma$, and Leu$^\delta$ methyl groups. The frequency of ^{13}C$-^{13}$C pairs is <5% for Ile, Val, and Leu, and is 20% for Ala. It was shown that, for these four methyl groups, pyruvate labeling improves the sensitivity over the random fractional approach by approximately 5-fold.[36] Other methyl groups, Thr$^\gamma$, Ile$^\delta$, and Met$^\varepsilon$, have low ^{13}C incorporation levels.

In another attempt to eliminate directly bonded ^{13}C$-^{13}$C pairs, LeMaster et al.[38] developed two complementary ^{13}C labeling schemes based on [1,3-^{13}C$_2$]- and [2-^{13}C]-enriched glycerols. When added to the growth medium in the presence of NaH^{12}CO$_3$ and NaH^{13}CO$_3$ to suppress the recycling of decarboxylated CO$_2$, the glycerols produced an alternating ^{13}C$-^{12}$C$-^{13}$C labeling pattern in the majority of amino acids. An exception is the branch sites of valine, leucine, and isoleucine that show high (>90%) levels of adjacent ^{13}C incorporation. This labeling procedure was applied to thioredoxin overexpressed in the *E. Coli* strain lacking succinate dehydrogenase and malate dehydrogenase. Combined with

Table 1. Isotope Labeling Schemes Used for Protein Side Chain Dynamics

labeling precursor	conc	labeling pattern	ref
mixture of 15% [2-^{13}C]acetate, 15% [1-^{13}C]acetate, and 70% [1,2-^{12}C$_2$]acetate	4 g/L	fractional	15
[3-^{13}C]pyruvate, sodium salt	0.3−0.4% (w/v)	Leu$^\delta$, Val$^\gamma$, Ile$^\gamma$, Ala$^\beta$: >90% ^{13}C Thr$^\gamma$, Ile$^\delta$, Met$^\epsilon$: low ^{13}C incorporation	36
D$_2$O/H$_2$O	50−65% (v/v)	methyls: CH$_3$, CH$_2$D, CHD$_2$, and CD$_3$ methylenes and methines: CH$_2$,CHD, CD$_2$, CH, and CD	16
[1,3-^{13}C$_2$]glycerol; [2-^{13}C]glycerol		^{13}C−^{12}C−^{13}C pattern	38
[3-^{13}C,3,3,3-D$_3$]pyruvate, [4-^{13}C,3,3,4,4,4-D$_5$]2-keto-butyrate, and D$_2$O	4 g/L, 0.2 g/L, and 98%	maximized yield of ^{13}CHD$_2$ groups in Leu$^\delta$, Val$^\gamma$, Ile$^{\gamma,\delta}$, and Ala$^\beta$	39
[γ1,γ2-^{13}C$_2$,α,β,-γ1,γ1,γ2,γ2-^{2}H$_6$]valine	0.23 g/L	^{13}CHD$_2$ (valines)	41
isotopically labeled α-ketoacids, [U-^{2}H]glucose, and D$_2$O	0.06−0.1 g/L (1 h prior to induction), 2 g/L, and 98%	Leu$^\delta$, Val$^\gamma$, Ile$^\delta$	31, 43, 52

fractional deuteration, this method produced (among other isotopomers) the isolated ^{13}C nuclei in the context of ^{13}CHD$_2$ and ^{13}CHD groups. Carbons bearing single protons were spectrally selected and used for ^{13}C-relaxation measurements of the backbone (Cα) and side chains of thioredoxin.

When the ^{2}H nucleus is used as a probe of dynamics of protein side chains, fractional deuteration can be easily combined with uniform ^{13}C enrichment, making it possible to carry out the resonance assignment work on the same protein sample. Fractional deuteration is accomplished by adjusting the D$_2$O/H$_2$O ratio to 50−65% (v/v) in the growth medium.[16] Two methyl isotopomers, ^{13}CH$_2$D and ^{13}CHD$_2$, could then be used for ^{2}H and ^{13}C relaxation studies, respectively.

Spectral selection of particular isotopomers in ^{2}H- and ^{13}C-based relaxation experiments reduces the concentration of spin labels contributing to the detected signal. In large molecular weight proteins, this considerably deteriorates the sensitivity of relaxation experiments. In addition, in ^{13}C relaxation studies, it is advantageous to maximize the yield of ^{13}CHD$_2$ isotopomers because the signals from ^{13}CH$_3$ groups cannot be filtered out completely by the appropriate pulse sequences. Two methods for maximizing the yield of ^{13}CHD$_2$ isotopomers have been reported. The first one makes use of [3-^{13}C,3,3,3-D$_3$]pyruvate, 50−60% deuterated at position 3, and [4-^{13}C,3,3,4,4,4-D$_5$]2-ketobutyrate, 62% deuterated at position 4.[39] The latter ^{13}C precursor ensures the labeling of the Ile$^\delta$ methyl group,[40] in addition to the standard methyl labeling pattern of [3-^{13}C]pyruvate (see Table 1). It was found that, when this labeling strategy is used in conjunction with uniform (98%) deuteration, the ratio of ^{13}CH$_3$ to ^{13}CHD$_2$ isotopomers does not exceed 8% for Ile$^\delta$ and 4% for all other ^{13}C-enriched methyl groups in an HIV-1 protease/inhibitor complex.[39] In another approach, Chaykovski et al.[41] chemically synthesized isotopically enriched valine, where both methyl groups were replaced by ^{13}CHD$_2$ isotopomers. Labeled valine residues were then incorporated into a 19 kDa mouse major urinary protein for ^{13}C relaxation measurements. Finally, selective biosynthetic labeling with ^{13}C$_1$-glucose[42] offers great potential in the investigation of relaxation phenomena in aromatic ring systems but has thus far not been exploited for fast time scale dynamics.

Special considerations have to be taken into account when labeling methyl groups of high-molecular-weight proteins (>40 kDa) for ^{2}H- and ^{13}C-based relaxation studies. The yield of the desired methyl labeling pattern has to be maximized to ensure optimum sensitivity. A high deuteration level of the entire protein and the absence of directly bonded ^{13}C$_{methyl}$−^{13}C spin pairs are necessary to take full advantage of recently developed resolution enhancement techniques.[43] This can be accomplished by using isotopically labeled α-ketoacids, which preferentially label Ile$^\delta$, Val$^\gamma$, and Leu$^\delta$ methyl positions. For a list of isotopically labeled α-ketoacids and their application to labeling of methyl positions in a 723-residue malate synthase G, the reader is referred to a recent review.[31]

A general chemical approach, termed "stereoarray isotope labeling" or SAIL, employs a range of stereoselective replacements of ^{1}H with ^{2}H in amino acid side chains through chemical synthesis and use of these precursors in the cell-free synthesis[44] of protein. Originally developed for the simplification and optimization of NMR spectra of large proteins,[45] the SAIL approach[46] has obvious potential for relaxation studies in proteins.

3.3. Experiments for Measurements of Autorelaxation and Cross-relaxation Rates

3.3.1. ^{13}C Relaxation Experiments for the Studies of Methyl Dynamics

The isotope labeling schemes designed for ^{13}C relaxation studies eliminate directly bonded ^{13}C−^{13}C pairs, making ^{13}C−^{1}H dipole−dipole interactions the primary relaxation mechanism in methyl groups. The smaller contribution coming from the chemical shielding anisotropy of the methyl carbon to the relaxation rates is usually neglected. A suite of experiments for the measurements of spin−lattice relaxation rate, R_1, spin−spin relaxation rate, R_2, and {^{1}H}−^{13}C NOE was developed for methyl groups.[33] Based on the pulse sequences for the measurements of relaxation properties of backbone ^{15}N−^{1}H spin pairs, these experiments incorporate modifications that take into account the complexity of spin interactions in ^{13}CH$_3$ groups.

Site resolution in ^{13}C relaxation experiments is achieved by collecting 2D ^{13}C−^{1}H chemical shift correlation spectra. ^{13}C nuclei are initially polarized via NOE exchange with protons that have been saturated by a train of 125° pulses. In the R_2 experiment, the first 90° pulse creates a transverse ^{13}C magnetization, which is allowed to relax during a variable time delay T that incorporates a Carr−Purcell−Meiboom−Gill (CPMG) pulse train with the spacing between the 180° pulses smaller than $1/J_{CH}$, where J_{CH} is the one-bond ^{13}C−^{1}H J-coupling constant. In the R_1 experiment, the relaxation delay T is simply a recovery period, followed by a 90° pulse

to create a transverse magnetization. The transverse ^{13}C magnetization is then allowed to evolve under the influence of chemical shift and is transferred to ^1H for detection via the reverse INEPT sequence.[33]

Two major issues considered in connection with the ^{13}C relaxation mechanism purity are the influences of cross-correlation effects and the parameters of the polarization transfer sequences on the measured relaxation rates. In $^{13}CH_3$ groups, the dominant interference effect is the cross-correlation between $^{13}C-^1H$ dipole−dipole interactions. Kay and Torchia considered the effects of cross-correlations for the methyl group motion described by a Woessner model.[28] It was found that, for a wide range of overall tumbling times τ_m (5−20 ns) and internal correlation times τ_e (15−65 ps), the contributions of cross-correlated relaxation to R_1 and the cross-relaxation rates (NOE) do not exceed 10% and 6−7%, respectively. This is because the cross-correlated spectral density function $J^{CH1,CH2}(\omega)$ changes its sign and is very small in the vicinity of $\tau_e\tau_m \sim 1/(4\omega^2)$. In the macromolecular limit of $(\omega\tau_m)^2 \gg 1$, $J^{CH1,CH2}(0)$ and the autocorrelated spectral density function $J^{CH}(0)$ make dominant contributions to the spin−spin relaxation rate, R_2, and are comparable. As a result, the decay of transverse magnetization becomes biexponential. Only when the relaxation time delay is very short could one safely assume that the relaxation of transverse magnetization is governed purely by the autocorrelated $^{13}C-^1H$ dipole−dipole interactions.

The effect of the parameters of polarization transfer sequences on the measured ^{13}C rates was analyzed in detail by Kay and Torchia.[47] It was found that appropriate setting of the reverse INEPT time delays was necessary to ensure equal contributions of the ^{13}C multiplet components to the measured relaxation rates. In addition, to minimize the cross-correlations between $^{13}C-^1H$ dipole−dipole interactions and $^{13}C-^1H$ dipole−dipole and ^{13}C chemical shielding anisotropy (CSA) interactions, a train of 125° ^1H pulses was applied during the relaxation period T in both R_1 and R_2 experiments. However, this method is unable to remove the effect of dipolar cross-correlations completely, and accurate R_2 values can be obtained only from the initial decay rates of the transverse magnetization.

Although successfully applied to a number of proteins, ^{13}C relaxation experiments have certain limitations that stem from the fact that it is necessary to use elaborate and often costly isotope labeling schemes to ensure the purity of the relaxation mechanism. A non-negligible contribution of $^{13}C-^1H$ dipole−dipole cross-correlated relaxation to R_2 is inevitable, unless $-^{12}C-^{13}CHD_2$ isotopomers are used. The "external" protons, while attenuating cross-correlation effects, provide additional relaxation pathways that are difficult to account for in a quantitative way. These problems were overcome by the development of ^2H relaxation techniques that can be applied to uniformly ^{13}C-enriched and fractionally deuterated proteins.

3.3.2. ^2H Relaxation for the Studies of Methyl and Methylene Group Dynamics

The advantage of using the ^2H nucleus as a probe of side chain dynamics comes from the strength of its quadrupolar interaction, which exceeds those of all other spin interactions by 1 to 2 orders of magnitude. The presence of one dominating relaxation mechanism makes ^2H relaxation data straightforward to analyze.

Pulse sequences designed to measure T_1 and $T_{1\rho}$ (spin−lattice relaxation time in the rotating frame) of ^2H nuclei in

$^{13}CH_2D$ isotopomers of methyl groups were developed by Kay and co-workers.[16] The relaxation rates of the three-spin $I_zC_zD_z$ and $I_zC_zD_y$ terms ($I = {}^1H$, $C = {}^{13}C$, and $D = {}^2H$) were measured in a modified $^{13}C-^1H$ HSQC experiment, which included the following polarization transfers and evolution periods:

$$^1H \xrightarrow{J_{CH}} {}^{13}C(t_1) \xrightarrow{J_{CD}} {}^2H(T) \xrightarrow{J_{CD}} {}^{13}C \xrightarrow{J_{CH}} {}^1H(t_2) \quad (36)$$
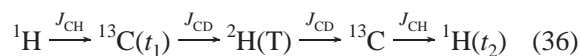
The initial polarization transfer from ^1H to the directly attached ^{13}C and the spectral filter that selects the signals of the $^{13}CH_2D$ isotopomers are followed by a carbon chemical shift evolution period t_1, implemented as a constant-time element with ^2H decoupling. The ^2H decoupling is turned off ~11 ms [equal to $1/(4J_{CD})$, where J_{CD} is a one-bond J-coupling constant between ^2H and ^{13}C] prior to the end of the evolution period. This generates the antiphase coherence that is subsequently converted to either $I_zC_zD_z$ or $I_zC_zD_y$ three-spin terms. $I_zC_zD_z$ or $I_zC_zD_y$ is allowed to relax during the time period T, which is either a recovery or spin-lock period. The relaxed three-spin terms are then transferred back to ^{13}C and finally to ^1H for detection. It is these multiple coherence transfers between fast relaxing spins that significantly limit this approach. This is particularly pertinent to the use of analogous experiments to measure deuterium relaxation in CHD methylene centers, where relaxation of all involved spins is inherently faster, making multiple coherence transfer even more problematic.[25] Approaches based on cross-correlated relaxation may be more effective (see section 3.4.1).

To address the question of relaxation mechanism purity, the contributions of various spin interactions to the measured relaxation rates were evaluated for the $^{13}CH_2D$ spin system.[16,48] Next to the ^2H quadrupole interaction, the major autorelaxation pathways are (i) $^1H-^1H$ dipole−dipole interactions, both intra-methyl and with "external" protons, and (ii) $^{13}C-^1H$ intra-methyl dipole−dipole interactions. If normalized to the contribution of the ^2H quadrupole interaction to the relaxation rates, the $^1H-^1H$ and $^1H-^{13}C$ autorelaxation rates are 19% and 7%, and they are 4% and 1% for $I_zC_zD_z$ and $I_zC_zD_y$, respectively. The effect of other autorelaxation mechanisms is negligible. The influence of $^1H-^1H$ and $^1H-^{13}C$ dipole−dipole interactions is eliminated by subtracting the decay rate of the two-spin order I_zC_z, measured in a separate experiment, from the $I_zC_zD_z$ or $I_zC_zD_y$ rates:

$$1/T_1(D_z) = 1/T_1(I_zC_zD_z) - 1/T_1(I_zC_z)$$

$$1/T_{1\rho}(D_y) = 1/T_{1\rho}(I_zC_zD_y) - 1/T_1(I_zC_z) \quad (37)$$

Numerical simulations indicated that, for a wide range of motion time scales and amplitudes, the contribution of cross-relaxation and cross-correlations (e.g., between the quadrupole and $^2H-^{13}C$ or $^2H-^1H$ dipole−dipole interactions) is negligible. Moreover, for the same range of motional parameters, the difference between the right and left sides of eq 37 does not exceed 3.0%.[48] This means that pure and readily interpretable ^2H relaxation rates can be obtained from the decay rates of the $I_zC_zD_z$, $I_zC_zD_y$, and I_zC_z terms measured in three separate experiments.

The ^2H autorelaxation methodology was subsequently expanded to include the relaxation measurements of three

other ^{2}H operators given by eqs 31: quadrupolar order $(3D_z^2 - 2)$, double-quantum magnetization D_+^2, and single-quantum antiphase magnetization $(D_+D_z + D_zD_+)$.[23] The experiments included the pulse sequence elements that selected the appropriate spin operators, and they allowed one to incorporate the decay of the two-spin order I_zC_z directly into the final rate measurement. It was shown that, similar to the cases of the ^{2}H T_1 and $T_{1\rho}$ experiments, pure ^{2}H relaxation rates could be obtained for $(3D_z^2 - 2)$ and $(D_+D_z + D_zD_+)$ terms. The double-quantum term D_+^2 has to be corrected for the contribution of dipole−dipole autorelaxation pathways. The methodology was applied to a 63-residue protein L, where five relaxation rates per deuteron were measured for 35 methyl sites at two magnetic field strengths. The rates satisfied the internal consistency relationships,[22] and there was a good agreement between the methyl order parameters and internal correlation times calculated using five rates (two fields) and two rates ($1/T_1$ and $1/T_{1\rho}$, one field). The experiments measuring $(3D_z^2 - 2)$, D_+^2, and $(D_+D_z + D_zD_+)$ relaxation are less sensitive than the original T_1 and $T_{1\rho}$ experiments and are likely not to be applicable to proteins exceeding 150 amino acid residues.

With five relaxation rates measured per deuteron and the three unknowns in eqs 30 and 31 representing the spectral density function $J(\omega)$ sampled at frequencies 0, ω_D, and $2\omega_D$, the mathematical problem of calculating the dynamic parameters becomes overdetermined even using data employed at a single field.[24]

When applied to high-molecular-weight proteins, ^{2}H relaxation experiments suffer from poor resolution and sensitivity. This is because during the first INEPT sequence the polarization is transferred from ^{1}H to rapidly relaxing outer components of the ^{13}C multiplet, and the rapidly and slowly relaxing ^{1}H components are mixed by the ^{13}C decoupling during acquisition. In addition, the efficiency of the subsequent INEPT transfers is diminished due to the unfavorable relaxation properties of the ^{13}C coherences, leading to poor sensitivity in the final 2D ^{1}H−^{13}C spectra. To extend the applicability of ^{2}H-based relaxation methods to proteins with molecular weights of ∼100 kDa, Kay and co-workers developed a transverse relaxation optimized spectroscopy (TROSY) version of the experiments as applied to the isolated ^{13}CH$_2$D groups.[49] In the TROSY version, polarization transfer pathways selectively utilize the slow-relaxing ^{13}C and ^{1}H multi-spin coherences, resulting in the marked improvement of resolution in the final 2D spectra. If relaxation losses are neglected, then the theoretical signal-to-noise in the CH$_2$D-TROSY experiment is $2\sqrt{2}$ lower compared to that of the HSQC experiment. Due to the competition between relaxation losses and TROSY compensation, the CH$_2$D-TROSY scheme becomes advantageous for proteins with τ_m values exceeding ∼25 ns.

The new methodology was validated using malate synthase G (MSG), a 82 kDa protein, labeled with ^{13}CH$_2$D at the Ile$^\delta$ positions. Relaxation properties of all ^{2}H coherences (eqs 30 and 31) with the exception of the double-quantum coherence were measured and found to obey self-consistency relationships.[22] In addition, a pulse sequence for the measurements of ^{2}H T_2 in isolated ^{13}CHD$_2$ groups was presented and applied to [^{13}CHD$_2$-Ile$^\delta$]MSG.[49] An excellent agreement was found between the methyl order parameters derived from ^{13}CH$_2$D and ^{13}CHD$_2$ groups in MSG.

3.3.3. On the Agreement between ^{13}C and ^{2}H Relaxation Measurements

A central question for the side chain dynamics is the general agreement between dynamic parameters obtained using different nuclear species located on the *same* functional group. If all relaxation mechanisms are properly taken into account, a consistent result, regardless of the reporter spins, should be obtained. This question was first taken up by Lee et al.,[50] who compared the order parameters and internal correlation times obtained from ^{2}H and ^{13}C autorelaxation studies of methyl groups in ubiquitin. The ^{2}H relaxation experiments included T_1 and $T_{1\rho}$ measurements carried out on a uniformly ^{13}C-enriched, fractionally deuterated ubiquitin; and ^{13}C relaxation experiments included T_1 and NOE measurements carried out on a [^{13}C-methyl]ubiquitin, prepared using [3-^{13}C]pyruvate as the sole carbon source. It was found that, when a simple "model-free" formalism, parametrized by the methyl rotation axis order parameter O^2_{axis} and the internal correlation time τ_{axis}, was used for the analysis of ^{13}C and ^{2}H relaxation data, the correlation between the ^{13}C- and ^{2}H-derived parameters was rather poor for O^2_{axis} and satisfactory for τ_{axis}. The agreement between ^{13}C- and ^{2}H-derived O^2_{axis} values somewhat improved when the extended "model-free" formalism, which included separation of the time scales for methyl rotation and methyl axis motion, was used to fit the ^{13}C data. Possible reasons for the observed discrepancy were the effect of "external" protons on the ^{13}C relaxation rates, uncertainties in the geometry and magnitude of spin interactions, and the effect of deuteration on protein dynamics.

This discrepancy was later resolved by Ishima et al.,[51] who carried out a similar study on the extensively deuterated, [^{13}C-methyl]-labeled HIV-1 protease/inhibitor complex. In the same protein sample, ^{13}CHD$_2$ isotopomers were used for ^{13}C, and ^{13}CH$_2$D isotopomers were used for ^{2}H relaxation measurements; in both cases, R_1 and R_2 ($R_{1\rho}$) relaxation rates were measured. A good agreement was obtained between the ^{2}H- and ^{13}C-derived dynamic parameters. Two factors proved to be crucial for obtaining consistent results: the availability of ^{13}C R_2 and the experimentally derived interaction constants. Since R_2 is very sensitive to O^2_{axis}, a combination of ^{13}C R_1 and R_2 is better suited for the calculation of O^2_{axis} than that of R_1 and NOE, provided the contribution of (i) cross-correlations and (ii) dipole−dipole interactions with "external" protons (and deuterons) to ^{13}C R_2 can be suppressed. ^{13}C−^{1}H dipolar cross-correlations were eliminated by spectrally selecting the ^{13}CHD$_2$ isotopomers, while extensive protein deuteration minimized the effect of "external" protons. In addition, the structure-based correction for the dipolar contributions of "external" ^{1}H and ^{2}H spins was applied to ^{13}C R_2. The interaction constants (such as ^{2}H quadrupolar and ^{13}C−^{1}H dipolar coupling constants) and methyl group geometry were constrained by the experimental relationships between the methyl quadrupolar, ^{13}C−^{13}C, and ^{13}C−^{1}H dipolar couplings obtained from the measurements of residual couplings in weakly aligned proteins. Unfortunately, reliable information on the time scale of motion appears to be lost by this approach.

^{2}H autorelaxation experiments are currently a method of choice, due to the purity of the relaxation mechanisms and straightforward interpretation of the relaxation data. However, as noted by Ishima et al.,[39] ^{13}C-relaxation could be advantageous for large proteins, where T$_{1\rho}$ of the ^{2}H nucleus would

be too short to be measurable. This has been subsequently shown to be the case. Tugarinov and co-workers[52] explored, among other issues, the agreement between the ^{13}C- and ^{2}H-derived methyl order parameters in the large MSG protein. Sub-nanosecond dynamics of Ile$^\delta$, Val$^\gamma$, and Leu$^\delta$ ^{13}CHD$_2$ groups was quantified using ^{13}C and ^{2}H relaxation techniques. When analyzing ^{13}C data, all mechanisms contributing to the observed relaxation behavior were explicitly taken into account. ^{13}C CSA values were measured in a separate experiment, while the dipolar contributions from the external ^{1}H and ^{2}H spins were estimated computationally. Good agreement between the ^{13}C- and ^{2}H-derived order parameters was obtained for all methyl groups. In this study, the ^{13}C experiments were found to be 3.3-fold more sensitive compared to the ^{2}H experiments.

3.4. Experiments for Measurements of Cross-correlated Relaxation Rates

3.4.1. Methylene Group Dynamics

Cross-correlated relaxation in proton-coupled ^{13}C spectra produces a different relaxation behavior of the ^{13}C multiplet components. This fact was exploited by Daragan and Mayo,[53] who measured the differential longitudinal relaxation in selectively ^{13}C-labeled methylene groups of the GXX-repeat hexapeptide. Using ^{13}C-detected inversion–recovery experiments, the initial relaxation rates of the inner and outer components of the ^{13}C triplet were measured and used in the calculation of the cross-correlated ^{13}C$-^1$H spectral density function:

$$J^{\mathrm{CH1,CH2}}(\omega_{\mathrm{C}}) = \frac{5}{6}\frac{r_{\mathrm{CH}}^6}{h^2\gamma_{\mathrm{C}}^2\gamma_{\mathrm{H}}^2}(W_{\mathrm{i}} - W_{\mathrm{o}}) \qquad (38)$$

where W_{i} and W_{o} are the initial relaxation rates of the inner and outer triplet components, respectively, h is Planck's constant, and the rest of the parameters are as defined in eq 15. The obtained value of the cross-correlated spectral density function could then be analyzed together with autocorrelated spectral densities to evaluate different motion models for the CH$_2$ groups. This experimental strategy relied on selective labeling and direct ^{13}C detection, making its application to proteins problematic. To combine site resolution with cross-correlated relaxation rate measurements, Ernst and Ernst[26] developed 2D pulse sequences that made use of polarization transfer mediated by cross-correlated relaxation in the laboratory and rotating frames. The idea was to encode the ^{1}H chemical shift in the indirect dimension, generate a pure $4\mathbf{S}_z\mathbf{I}_{1z}\mathbf{I}_{2z}$ order, let it cross-relax during the mixing period to yield $\mathbf{S}_z$, and directly detect the resulting magnetization with a "read" pulse under the conditions of ^{1}H decoupling. This method is applicable to ^{13}CH$_2$ and ^{13}CH$_3$ groups, and its rotating-frame variant was applied to ubiquitin. Based on the phase of the cross-peaks in 2D chemical shift correlation spectra, the experiment allows one to distinguish between restricted and unrestricted motions of CH$_2$ groups in isotropically tumbling molecules. The sensitivity of this method is a concern since the transfer efficiencies are rather low and the ^{13}C nucleus is used for detection.

Two-dimensional ^{1}H-detected pulse sequences for the measurements of cross-correlated spectral densities in methylene groups of proteins were reported recently by Mayo's group.[27] Two separate experiments with the identical number of relaxation time increments were recorded, mea-

suring the longitudinal autorelaxation rate, W_{C}, and the cross-correlated relaxation rate of the outer triplet components, W_{o}. In both experiments, the relaxed and chemical-shift-encoded ^{13}C coherences were transferred to ^{1}H for detection via the inverse INEPT sequence. The difference between the measured rates can be related to cross-correlated spectral density using an equation analogous to eq 38. The method was validated using a selectively ^{13}C-enriched hexapeptide and then applied to uniformly ^{13}C-enriched 56-residue protein GB1. Based on the ratio of the cross-correlated and autocorrelated spectral densities calculated for the majority of protein sites, the C$^\alpha$ methylene carbons of glycines were found on average to be less motionally restricted than C$^\beta$ and C$^\gamma$. A motion restriction map[29] was constructed for GB1 and analyzed in terms of correlated and anticorrelated motions.

It has been demonstrated for moderately sized proteins that interference phenomena between dipole–dipole interactions for the transverse magnetization can be exploited to obtain information about the dynamics of protein side chains. For a 59-residue drkN SH$_3$ domain, Yang et al. compared the results of the ^{2}H autocorrelated and ^{13}C cross-correlated relaxation experiments that probed the dynamics of C$^\beta$ (and glycine C$^\alpha$) methylene groups in protein side chains.[25] The cross-correlated relaxation experiment was based on a 3D CBCA(CO)NH pulse sequence that correlates amide nitrogen and proton chemical shifts with those of the C$^\alpha$ and C$^\beta$ carbons of the preceding residue. No ^{1}H decoupling was applied during the constant-time carbon chemical shift evolution period. As a result, ^{13}C signals of methylene groups gave rise to a J-coupled triplet, in which the deviations of the intensities from the 1:2:1 ratio could be related to the dipole–dipole ^{13}C$-^1$H cross-correlated relaxation rate as follows:[25]

$$\Gamma^{\mathrm{CH1,CH2}} = -\frac{1}{4T}\ln\frac{4I_{\alpha\alpha}I_{\beta\beta}}{(I_{\alpha\beta+\beta\alpha})^2} \qquad (39)$$

where T is the duration of the constant-time period; and $I_{\alpha\alpha(\beta\beta)}$ and $I_{\alpha\beta+\beta\alpha}$ are the intensities of the outer and inner triplet components, respectively. The dipole–dipole cross-correlated relaxation rate of the transverse magnetization depends on the values of spectral density functions sampled at frequencies 0 and ω_{C} (see eq 35). Assuming a specific form of the cross-correlated spectral density function[28] and using the effective correlation times obtained from ^{2}H-based experiments, a set of order parameters O_{HCH}^2 was calculated for the drkN SH3 domain. A simultaneous analysis of O_{HCH}^2 and O_{CD}^2, obtained from autorelaxation ^{2}H experiments, made it possible to evaluate plausible motion models for methylene groups of protein side chains.

This methodology was later extended to *all* methylene groups in protein side chains, making use of a 3D CC(CO)-NH experiment that correlates amide nitrogen and proton chemical shifts with those of all side chain carbons of the preceding residue.[54] The normalized cross-correlation rate S', calculated as a ratio of the observed cross-correlated relaxation rate $\Gamma^{\mathrm{CH1,CH2}}$ and the calculated rate in the rigid limit $\Gamma^{\mathrm{CH1,CH2}'}$, was used to characterize the dynamics of the majority of methylene sites in a 131-residue intestinal fatty acid binding protein. This method allows one to accurately measure $\Gamma^{\mathrm{CH1,CH2}}$, if the molecular tumbling is isotropic, τ_{m} does not exceed 8 ns, and the macromolecular limit condition is satisfied.

Transverse cross-correlated relaxation experiments applied to the studies of methylene group dynamics offer the following advantages when applied to small proteins: (i) there is no need for deuteration, and uniformly $^{13}C,^{15}N$-enriched protein samples can be used; (ii) there is little uncertainty about the orientation and magnitude of the dipolar coupling tensors; and (iii) there is no scaling of the interference effect with the static magnetic field. In addition, spectral resolution is greatly enhanced by a 3D acquisition mode, and the relaxation rates can be obtained from a single 3D experiment. The disadvantages include (i) possible phase distortions of carbon multiplets due to strong coupling effects between the carbons of protein side chains and (ii) low polarization transfer efficiencies in TOCSY-based experiments such as CC(CO)NH.

3.4.2. Methyl Group Dynamics

Similar to the case of methylene groups, cross-correlated relaxation rates of $^{13}CH_3$ groups in the intestinal fatty acid binding protein were measured using a 3D CC(CO)NH experiment.[55] Intensities of the ^1H-coupled ^{13}C quartet components were used to calculate $\Gamma^{CH1,CH2}$, as well as $\Gamma^{C,CH}$, the cross-correlated relaxation rate between the $^{13}C-^1H$ dipole−dipole interaction and ^{13}C CSA. Assuming that the CSA tensor is axially symmetric, with one of the principal axes coinciding with the symmetry axis of the methyl group, it was possible to obtain an estimate of the tensor anisotropy from the measured $\Gamma^{C,CH}$. The average anisotropy was found to be 26.0 ppm, with the standard deviation of 5.1 ppm, which is in good agreement with 25 ppm, a value normally used for ^{13}C relaxation studies.

Information about methyl group dynamics can also be obtained from ^{13}C multiple-quantum experiments reported recently by Tugarinov et al.[56] In the indirect dimension of the double quantum (DQ) or zero quantum (ZQ) $^{13}C-^1H$ spectra, an isolated $^{13}CH_3$ group gives rise to a triplet, whose inner and outer components show very different relaxation behavior in highly deuterated, methyl-protonated proteins. The inner components relax slowly due to the cancellation of autocorrelated and cross-correlated dipole−dipole relaxation pathways, in what is known as the TROSY effect.[57,58] In contrast, the outer components relax very fast and can be detected only in small proteins. The difference between relaxation properties of ZQ and DQ ^{13}C triplets is directly related to the cross-correlated relaxation rate $\Gamma^{CH,HH}$ between intra-methyl $^1H-^1H$ and $^{13}C-^1H$ dipole−dipole interactions. Pulse sequences for the measurements of the differential ZQ/DQ relaxation for inner and outer triplet components were developed and applied to a highly deuterated, $[^{13}C\text{-Ile}^\delta]$-protein L.[56] O^2_{axis} values were calculated from the obtained values of $\Gamma^{CH,HH}$ under the assumption that $J^{CH,HH}(0)$ makes a dominant contribution to the relaxation rate, and they were found to be in excellent agreement with O^2_{axis} values obtained from ^2H autorelaxation experiments. This agreement should not hold for the proteins with overall tumbling times shorter than 5 ns, since the assumption about the dominant contribution of $J^{CH,HH}(0)$ to $\Gamma^{CH,HH}$ becomes invalid.

4. Describing the Motion

4.1. Model-free Form of the Spectral Density

Thus far, we have largely ignored the details of the spectral density. In the context of solution NMR relaxation in

macromolecules, the spectral density contains information about fluctuations of the interaction vector of interest due to both motion within the molecular frame and motion involving the entire macromolecule, i.e., global molecular reorientation. An unfortunate but inescapable feature of the physics of NMR relaxation is the degeneracy of the underlying motion. Model-specific analyses of relaxation phenomena, while useful and often illuminating, constantly run the risk that the resulting physical picture is neither unique nor fundamentally certain, except in very special circumstances. A full decade prior to the introduction of robust methods designed to faithfully measure relaxation phenomena in macromolecules in solution (*vide supra*), Lipari and Szabo (L−S) developed an approach to capture the unique dynamical information available in a uniform and robust way.[59,60] Termed the "model-free" approach, this analytical strategy has proven remarkably useful and has dominated the analysis of NMR relaxation in macromolecules. Here we will present a compact description of the model-free treatment.

Ultimately, we are interested in the motion of an "interaction vector" within a macromolecule tumbling in isotropic solution. The spectral density defining NMR relaxation parameters (*vide supra*) is fundamentally defined by the cosine Fourier transform of the time correlation function that describes the fluctuations that modulate spin interactions. A key step in the L−S treatment is the assumption that internal motion and global macromolecular tumbling are independent, a condition that is generally robust when their time scales are significantly different. In this case, the autocorrelation function describing the time dependence of the nuclear spin interaction vector is simply

$$C(t) = C_0(t)\, C_I(t) \tag{40}$$

$$C_I(t) = \langle P_2(\hat{\mu}(0)\cdot\hat{\mu}(t))\rangle \tag{41}$$

Here $C_0(t)$ describes the global macromolecular reorientation. $C_I(t)$ describes the autocorrelation function for internal motion and is the ensemble average of the second-order Legendre polynomial (P_2) of the time-dependent dot product of the unit interaction vector $\hat{\mu}$. Lipari−Szabo insightfully point out that if the motion is Markovian, which is to say diffusive or jumplike without memory, then the internal correlation function can always be expressed as a weighted sum of exponentials with characteristic time constants, τ_i.

$$C_I(t) = \sum a_i e^{-t/\tau_i} \tag{42}$$

The mathematical structure of the internal correlation time suggests its approximation as

$$C_I^{L-S}(t) = O^2 + (1 - O^2)e^{-t/\tau_e} \tag{43}$$

where τ_e is an effective correlation time and O^2 is termed the square of the so-called generalized order parameter, originally S^2 and renamed here O^2 to avoid confusion with entropy (S). The O^2 parameter then represents the magnitude of the decay of the autocorrelation function due to internal motion (Figure 1). The generalized order parameter or, equivalently, the limiting value of the internal correlation function can also be defined within a spherical harmonic basis set as
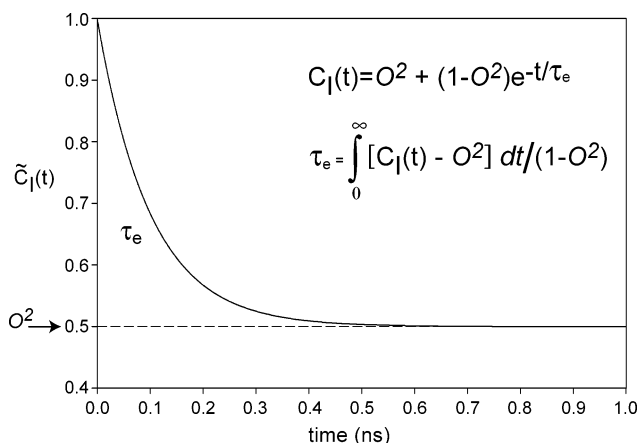
Figure 1. Schematic illustration of the Lipari–Szabo model-free internal autocorrelation function describing the motion of a nuclear spin interaction vector within the molecular frame of an isotropically tumbling macromolecule.[60] The square of the generalized order parameter (O^2) defines the contribution of internal motion to the decay of the autocorrelation function. The effective correlation time (τ_e) is defined as the normalized area under the internal correlation function. This particular example was simulated with O^2 of 0.5, τ_e of 200 ps, and an isotropic global reorientation correlation time (τ_m) of 10 ns. Note, the original Lipari–Szabo treatment utilizes the symbol S to denote the generalized order parameter. To avoid confusion with the similar symbol corresponding to entropy, we shall employ O throughout to denote the generalized order parameter.

$$O^2 \equiv C_I(\infty) = \sum_{m=-2}^{2} |\langle C_{2m}(\Omega) \rangle| \qquad (44)$$

where $C_{2m}(\Omega)$ are the modified spherical harmonics of Brink and Satchler.[61]

The effective correlation time is defined as the normalized area under the Lipari–Szabo internal correlation function, i.e.

$$\tau_e \equiv \int_0^{\infty} (C_I^{L-S}(t) - O^2)\, \mathrm{d}t/(1 - O^2) \qquad (45)$$

The approximation represented by eq 43 is exact as $t \rightarrow 0$ and $t \rightarrow \infty$. Indeed, simulations indicate that this treatment is remarkably accurate if the effective correlation time is appropriately defined. O^2 therefore becomes a model-independent measure of the degree of angular order of the interaction vector and represents the limiting decay of the autocorrelation function due to internal motion. The definition of the effective correlation time as the area under $C_I^{L-S}(t)$ emphasizes that it is not a physically meaningful time constant for internal motion. Rather, the effective correlation time depends both on the time constants *and* on the amplitude of internal motion. It is also important to emphasize that the L–S form of the internal correlation function does not correspond to a simple two-term truncation of eq 42. In a related vein, the effects on model-free parameters that result from violation of the decoupling approximation have been explored.[62]

Other functional forms, corresponding to qualitatively different motion, are also plausible. Indeed, motion involving "gated diffusion" has been shown to give rise to a stretched exponential relaxation behavior. For some time it has been appreciated that slower (i.e., microsecond) nonequilibrium protein fluctuations usually assume complex time dependencies that are often conveniently described by stretched

exponentials.[5,63] Theoretical treatments of the gated diffusion problem have illuminated the origin of this class of polymer motion.[64,65] In several respects, the presence of this type of motion in the nanosecond time regime would violate the assumptions of the Lipari and Szabo treatment and could lead to significant deviation from the underlying Pade approximation.[66] Distinguishing between the various potential internal correlation functions is often reduced to detailed statistical analyses and requires a significant amount of relaxation data in order to be meaningful. Bayesian statistics appear to be particularly useful in this regard.[67] Thus far, there are very few instances where the model-free treatment appears to give a qualitatively misleading view of the motion underlying relaxation.

If we consider the global reorientation of the macromolecule to be isotropic with a characteristic time constant τ_m, then eq 40 becomes

$$C^{L-S}(t) = \frac{1}{5}O^2 e^{-t/\tau_m} + \frac{1}{5}(1 - O^2)e^{-t/\tau} \qquad (46a)$$

where $\tau^{-1} = \tau_m^{-1} + \tau_e^{-1}$. The corresponding Lipari–Szabo spectral density, derived from the real Fourier transform of eq 46a, is then

$$J^{L-S}(\omega) = \frac{2}{5}\left[\frac{O^2 \tau_m}{1 + \omega^2 \tau_m^2} + \frac{(1 - O^2)\tau}{1 + \omega^2 \tau^2}\right] \qquad (46b)$$

In some cases, motion of the interaction vector involves contributions from simple bond vibrations and librations, such as those occurring during dipole–dipole relaxation of ^{15}N or ^{13}C by attached hydrogen(s). In this situation, time-dependent changes in bond geometry can enter via the dipolar coupling constant in eq 15 and the L–S internal correlation function must be modified as follows:[68]

$$\tilde{C}_I(t) = \left\langle \frac{P_2(\hat{\mu}(0)\cdot\hat{\mu}(t))}{r^3(0)\, r^3(t)} \right\rangle \qquad (47)$$

Formally, the generalized order parameter and the bond length averaging are no longer separable. Some effort has gone into estimating the effective bond length and thereby allowing for its removal from eq 47 and incorporation into the dipolar coupling constant. For example, Ottiger and Bax[69] have established that, due to more complicated motion of the attached hydrogen, an effective amide N–H bond distance of 1.04 Å is more appropriate than the value of 1.02 Å commonly used up to that time. This is the origin of the apparent inflation in generalized order parameters for protein amide N–H vectors subsequently reported in the literature.

4.2. Rotational Diffusion

Model-free analysis of relaxation data relies on the explicit separation of time scales for the overall and internal motions in a protein molecule, with both motions represented by their own correlation functions. In the general case of anisotropic reorientation, the expression for the correlation function for overall rotational motion, $C_O(t)$, represents a linear combination of exponential terms.[70]

$$C_O(t) = \sum_{i=1}^{5} A_i e^{-t/\tau_i} \qquad (48)$$

where the time constants τ_i and coefficients A_i depend on the principal components of the rotational diffusion tensor and the relative orientation of the diffusion tensor and the relaxation vector. The expression is reduced in higher symmetry cases, giving rise to three and one exponential terms for the axially symmetric and isotropic tumbling, respectively. Since the influence of motional anisotropy on relaxation parameters could be misinterpreted as the presence of slow motions,[71] knowledge of the rotational diffusion tensor is crucial for the reliable interpretation of NMR relaxation data.

The rotational diffusion tensor, **D**, can be obtained experimentally from the amide backbone relaxation data, such as R_1, R_2, and {^{1}H}$-^{15}$N NOE, provided that either the NMR spectrum or crystal structure of the protein of interest is available. Two approaches are usually employed, one based on the calculation of local diffusion coefficients D_i,[72,73] and the other based on the direct fitting of the R_2/R_1 ratios.[74,75]

In the local D_i approach, individual values of "local" tumbling times τ_{ci} are obtained for each ^{15}N$-^1$H pair by fitting either the isotropic Lipari−Szabo function, that also includes the part responsible for local motions,[72] or the R_2/R_1 ratios.[73] For fast, small-amplitude internal motions, R_2/R_1 ratios to a good approximation depend only on the spectral densities for the global motion calculated as a Fourier transform of eq 48. This method is made more robust if R_2R_1 product is used to filter out sites that are contaminated by contributions from chemical exchange.[76] For small anisotropies of the diffusion tensor, the local diffusion coefficients D_i, obtained as $D_i = \frac{1}{6}\tau_{ci}$, have a quadratic form and can be used for the calculation of the tensor matrix in the molecular frame. The resulting matrix is then diagonalized to obtain the principal values of the diffusion tensor **D** and the orientation of its principal axes relative to the molecular frame.

Parameters of the diffusion tensor **D** can also be directly fitted to the R_2/R_1 ratios of ^{15}N$-^1$H pairs, as was demonstrated in the backbone dynamics study of *trp* repressor[74] and the rotational anisotropy study of ubiquitin.[75] For ubiquitin, it was shown that an axially symmetric rotational diffusion tensor is fully consistent with the ^{15}N relaxation data and that increasing the number of adjustable parameters in the case of an asymmetric **D** tensor does not result in a statistically significant improvement of the fit. Computational approaches toward the determination of rotational diffusion tensors of proteins with known structure are reviewed elsewhere.[77,78]

4.3. Quantitative Analysis

The first comprehensive application of a global model-free treatment of relaxation in a sizable polypeptide system was that of the immunosuppressive cyclosporine A.[79] Many of the numerical strategies developed there are still employed today. The Lorentzian form of the L−S spectral density is somewhat featureless, making fitting of experimental data with standard regression methods problematic. The error surface is globally smooth but locally rough. Global fitting with normalized weighted error analysis over a discrete parameter grid proves to be the most efficient and reliable method for obtaining dynamical parameters.[79] Though a computational challenge then, the advent of fast computers now makes this approach trivial. For either isotropic or anisotropic (when the structure is known) tumbling, fitting can be globally linked.[79] For N-sites in an isotropically
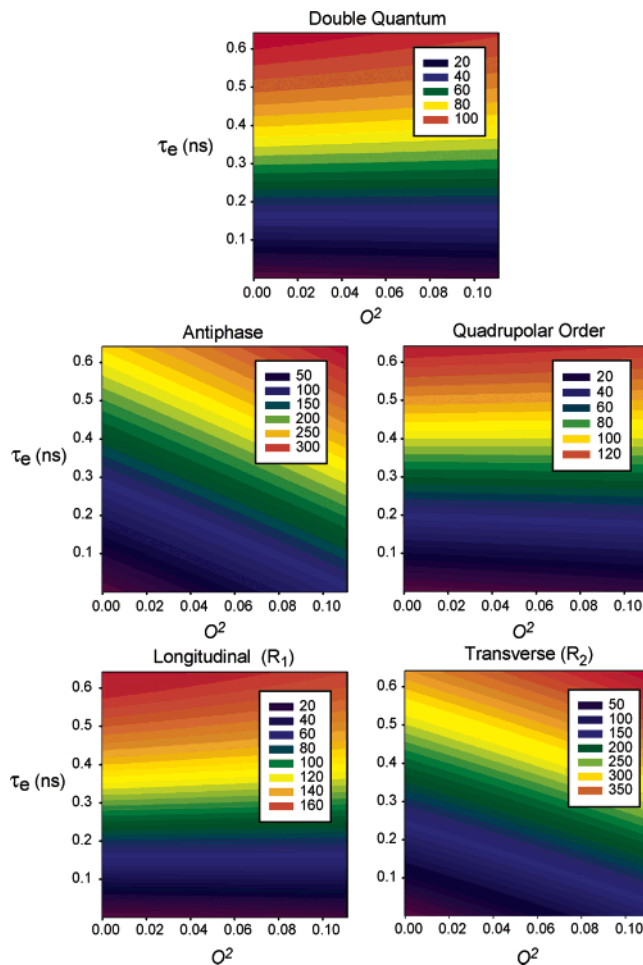
Figure 2. Motional dependence of the deuterium relaxation parameters observable using the two-dimensional ^{1}H$-^{13}$C sampling approach of Kay and co-workers.[23] Shown are simulations of the five deuterium relaxation parameters in methyl groups as a function of various model-free descriptors of internal motion. Note that the raw squared generalized order parameter is given, which is divided by 0.111 to give the derived O^2_{axis} parameter. Inset rates are given in s^{-1}.

tumbling macromolecule, this represents $2N + 1$ unknowns, requiring measurement at multiple frequencies [multiple values of $J^{\text{L−S}}(\omega)$] and/or of multiple relaxation parameters in order to be sufficiently overdetermined to allow for proper error analysis. Care needs to be taken in the choice of relaxation parameters to measure. One needs to avoid employing relaxation parameters with similar dependence upon model-free parameters. Figure 2 shows simulations of the model-free parameter dependence of the five deuterium relaxation parameters obtainable using the suite of experiments introduced by Kay and co-workers.[23] One can easily see why use of all five observables can robustly yield reliable model-free parameters while use of, say, the so-called double-quantum and quadrupolar order relaxation parameters alone might not. Similar issues arise in the choice of nucleus for sampling specific time scales of motion.[66]

Quite apart from concerns relating to the accurate measurement of relaxation parameters (*vide supra*), one needs to be conscious of the limitations of the observables themselves to report on internal motion. Uncertainties in the values of fundamental parameters such as effective bond distances, in the case of dipole−dipole relaxation between attached nuclei, the quadrupolar coupling constant, in the case of deuterium relaxation, and the orientation and breadth

of the chemical shift tensor, in the case of chemical shift anisotropy relaxation,[80] can significantly affect the reliability of obtained model-free parameters. Though good estimates are available for all of these fundamental parameters, their uncertainty needs to be projected onto obtained model-free relaxation parameters. Indeed, it was shown quite early that the uncertainty of the breadth of the chemical shift tensor at amide N−H can dwarf the uncertainty introduced by the imprecision of the measurement itself.[81]

In some cases, the simple model-free treatment fails and an extended form that incorporates time scale separation for internal motion faster than overall tumbling is often employed.[82,83] Statistical tests have been introduced to distinguish between various limiting cases of the simple and extended model-free spectral densities in various limits.[84,85] In all cases, one has to be aware that extreme values of one model-free parameter can reduce the obtained value of another to simply fitting the noise in the data. A good example is that when O^2 tends to unity, the effective correlation time becomes unreliable since its influence in the regression is scaled by $(1 - O^2)$ (see eq 46b).[79]

Finally, it is important to note that the $P_2(\cos \theta)$ dependence of the effects of motion on relaxation is highly nonlinear (see eq 44). Indeed, it can lead to situations where motion that is present is not manifested in the relaxation. An example would be motion about the interaction vector which results in no net effect, i.e., $\langle P_2(\cos \theta) \rangle = 1$. This is an important qualification that needs to be constantly kept in mind.

4.4. Spectral Density Mapping

The model-free treatment presumes that the simple Lorentzian spectral density defined in eq 46b is sufficiently accurate to capture the essential elements of the underlying motion.[59,60] Numerical simulations and experimental results largely bear this out.[59,60] Nevertheless, an alternate approach is to directly solve for the spectral density and do so without assumption of its functional form. This approach, pioneered by Peng and Wagner,[86,87] has been termed "spectral density mapping" and provides a useful assessment of the nature of the spectral density function defining NMR relaxation phenomena. It has been employed in the context of deuterium relaxation in side chains.[24] Generally, in the absence of contaminating relaxation mechanisms or methodological limitations, the spectral densities revealed by this approach appear to be largely Lorentzian and compatible with the model-free treatment.

4.5. Model-Dependent Analysis

Prior to the introduction of the Lipari−Szabo model-free approach, the usual strategy was to employ specific dynamical models to extract motional information from NMR relaxation. Possibly because of the paucity of data available in complex systems such as proteins, this approach suffered from the lack of sufficient experimental information to result in a unique physical insight and thus it gave way to the model-free approach. Nevertheless, specific models are highly useful, especially in situations where multiple probes are available and/or a great deal is known about the precise character of the underlying motion.

There is a rich and long history of the development of specific motional models in the context of NMR relaxation phenomena. Particularly relevant to side chain motion are those models that seek to describe the influence of rotations about multiple torsion angles on the relaxation of attached nuclei; for examples, see refs 170−177. Both free and restricted diffusion and jump models have been extensively explored. These treatments have been comprehensively discussed in an elegant review by Daragan and Mayo.[88] Though powerful, these detailed models, as implied above, somewhat overwhelm the experimental methods currently available. This is mostly due to the inability to spectrally resolve methylene centers in amino acid side chains of proteins of significant size, i.e., larger than 100 amino acids.

Another class of specific models refers to modeling the statistical distribution of states explored by the amino acid side chain and the NMR spy attached to it. This approach provides, in principle, direct access to the underlying thermodynamics of the protein conformation ensemble as expressed by motion on the NMR relaxation time scales. One such model is the Gaussian axial fluctuation (GAF) model proposed by Brüschweiler and Wright.[89] In this treatment, the squared generalized order parameter O^2 is expressed as a function of the sum of the second moments (or variances) $\sigma^2_{Y_{2m}}$ of the second-order spherical harmonics Y_{2m}:

$$O^2 = 1 - \frac{4\pi}{5} \sum_{m=-2}^{2} \sigma^2_{Y_{2m}} \qquad (49)$$

The calculation of the second moments $\sigma^2_{Y_{2m}}$ requires the knowledge of the angular probability functions. In the GAF model, the axial angle φ is assumed to be distributed according to the Gaussian function:

$$p(\varphi) = (2\pi\sigma_\varphi^2)^{-1/2} \exp(-\varphi^2/2\sigma_\varphi^2) \qquad (50)$$

For the motional model where (i) the diffusion of the relaxation vector occurs on the surface of a cone having a semiangle θ and (ii) the angle φ is described by the GAF, the following expression for O^2 is obtained:

$$O^2 = 1 - 3 \sin^2 \theta \left\{ \cos^2 \theta (1 - e^{-\sigma_\varphi^2}) + \frac{1}{4} \sin^2 \theta (1 - e^{-4\sigma_\varphi^2}) \right\} \qquad (51)$$

This expression for O^2 shows the correct limiting behavior of the Woessner limit when the variance σ_φ^2 is very large.

Subsequently, a variety of other azimuthally symmetric potentials have been utilized in the context of interpreting dynamical parameters in terms of the underlying thermodynamics. These include free diffusion in a cone, corresponding to an infinite square well, and a range of power, step, and conditional probability potentials.[90−94]

5. Insights into Fast Side Chain Motion Provided by NMR Relaxation

Historically, the initial efforts ito employ two-dimensionally sampled carbon relaxation, e.g. refs 15, 35, and 38, to characterize side chain motion in proteins of significant size ultimately gave way to use of methyl deuterium relaxation. Since their introduction a decade ago,[16] experiments designed to employ deuterium NMR relaxation phenomena have become the dominant means for the characterization of methyl group dynamics in proteins. This is largely due to the clarity of the underlying relaxation mechanism.[16] At the

Table 2. Database of Proteins Characterized by Methyl Deuterium Relaxation

temp (°C)	protein ligand/mutation	PDB code[d]	dynamics ref
20	HIV-1 protease	1QBS	51
	DMP323	1KJ7	123
	adipocyte lipid binding protein	1LIB	124
	muscle fatty acid binding protein	1HMT	124
25	protein L	1HZ6	125
	A20V, F22L		
	Cdc42Hs (GDP)	1AJE	115
	effector PAK PDB46 peptide	1EES	
	GMPPCP (GTP analogue)		
	tenascin, third fnIII	1TEN	102
	fibronectin, tenth fnIII	1FNF	102
	Fyn SH3	1SHF	126
	F20L, F20V		127
	hPTP1e PDZ2 domain	1GM1[a]	122
	RA-GEF2 peptide	1D5G	
27	U1A	1FHT	128
28.5	dihydrofolate reductase (folate)	1RX7	129
	folate and NADP$^+$	1RX2	
30	α_3D	2A3D	101
	ferrocytochrome c_2 (oxidized)	1C2R	130
	phospholipase Cγ1 SH2		131
	pY10121 PDGFR peptide	2PLE	132
	SAP SH2	1D1Z	133
	Y281 peptide	1D4T	
	pY281 peptide	1D4W	
	NSyp SH2	1AYD	134
	pY1172 peptide	1AYA[b]	
	protein G B1	2GB1	118
	T53A, T53D, T53H, T53I, T53L		
	T53M, T53S, T53W, T53V		
	ubiquitin	1UBQ	50
	1D7 (designed core mutant)	1UD7	135
30.9	troponin C	5TNC	136
35	flavodoxin (oxidized)	1FLV	100
	major urinary protein [Val only]	1QY0	137
	2-methoxy-3-isobutylpyrazine	1QY1	
	2-methoxy-3-isopropylpyrazine	1QY2	
	calmodulin	3CLN	106
	calmodulin/smMLCK peptide	1CDL	106
	D95N, D58N, M124L, E84K		117
37	eglin c (pH 7)	1CSE[c]	138
	pH 3	1EGL	
	V14A, V54A		139

^{a} The mouse hPTP1E PDZ2 isoform (94% homologous) was used to model the free state of the human protein. ^{b} The Nsyp SH2/pY1009 complex is used to model the NSyp SH2/pY1172 complex. ^{c} The eglin c/Carlsberg structure at neutral pH is used to model free eglin c at pH 7. ^{d} When a PDB code is not given, there is not a structure for the corresponding protein. The relaxation data was therefore not employed in structure-dependent analyses (e.g. Figure 3) but was used in structure-independent analyses reported here (e.g. Figure 7).

time of writing, approximately two dozen proteins of significant size, some in more than one functional state, have been characterized using these methods (Table 2). In contrast, there have been few cases of deuterium or carbon relaxation in methylene centers in proteins of significant size, with the latter studies compromised somewhat by relaxation by remote ^{1}H spins, as discussed above. In addition, the fast sub-nanosecond dynamics of aromatic rings in proteins of significant size have not really been studied at all. Accordingly, our view of side chain motion in proteins is largely dominated by that provided by deuterium relaxation in methyl groups. We shall focus on this view with the clear admission that it is a limited one and should be greatly expanded as soon as emerging methods allow the investigation of relaxation at other more challenging sites within proteins.

5.1. Absence of Simple Structural Correlates and Side Chain Motion

It can now be confidently stated that the amplitudes of sub nanosecond motion of methyl-bearing amino acid side chains are heterogeneously distributed throughout the protein macromolecule. The observed distribution of O^2_{axis} parameters does not follow from an intuitive view of proteins as densely packed and rigid polymers. Indeed, despite many instances in the literature where it is generally asserted that side chain rigidity should (roughly) correlate with depth of burial or packing density or inversely correlate with solvent accessible surface area, there is, in fact, no such correlation. There is essentially no correlation between the measured generalized order parameters for methyl groups in proteins and their depth of burial, their local packing density, or their solvent accessible surface area (Figure 3). Indeed, methyl groups at the surface of proteins can be among the most rigid in the molecule. Similarly, buried methyl groups, centered at the core of these proteins, can be among those with the largest angular disorder on the sub-nanosecond time scale. Examples are drawn from the complex between calcium-saturated calmodulin and a target domain to illustrate this perhaps counter-intuitive point (Figure 4). The observations summarized by Figure 3 clearly suggest that none of these primitive structural parameters can be used to predict the local dynamics of proteins in a simple way and that more subtle context-dependent determinants may exist.

It is also important to note that the crystallographic B-factor is often employed to highlight extreme variations in disorder, but it too is not a strong general predictor of the methyl generalized order parameter (Figure 3). In retrospect, this is not surprising since crystal structures are typically determined at cryogenic temperatures whereas methyl order parameters are obtained at significantly higher temperatures where liquid NMR spectroscopy is carried out. Temperature significantly affects motion manifested in methyl side chain order parameters.[95] In addition, the simple B-factor contains nondynamic contributions such as lattice disorder and, in nonideal cases, incorporates refinement error.

The inability of simple structural correlates to accurately predict the experimentally determined amplitude of methyl group dynamics in proteins is clear. The fact that there is essentially no general correlation of the amplitude of motion of methyl groups with the primitive descriptors of accessible surface area, depth of burial, or packing density suggests that motion is highly context dependent and that the rules governing these motions remain to be illuminated. Given that under the best of circumstances current molecular dynamics simulations capture only the slight majority of the variations of methyl group generalized order parameters,[96−98] the experimental characterization of fast side chain dynamics remains a prerequisite for the definitive characterization of internal protein motion. This strongly promotes continued study of the dynamics within proteins using NMR-based methods.

5.2. Distributions of the Amplitude of Fast Side Chain Motion

The distribution of the generalized order parameters for the methyl group symmetry axes in the calmodulin/smMLCKp complex is remarkable for its distinct clustering into three apparent classes of motion. The trimodal distribution is emphasized in the temperature dependence of the
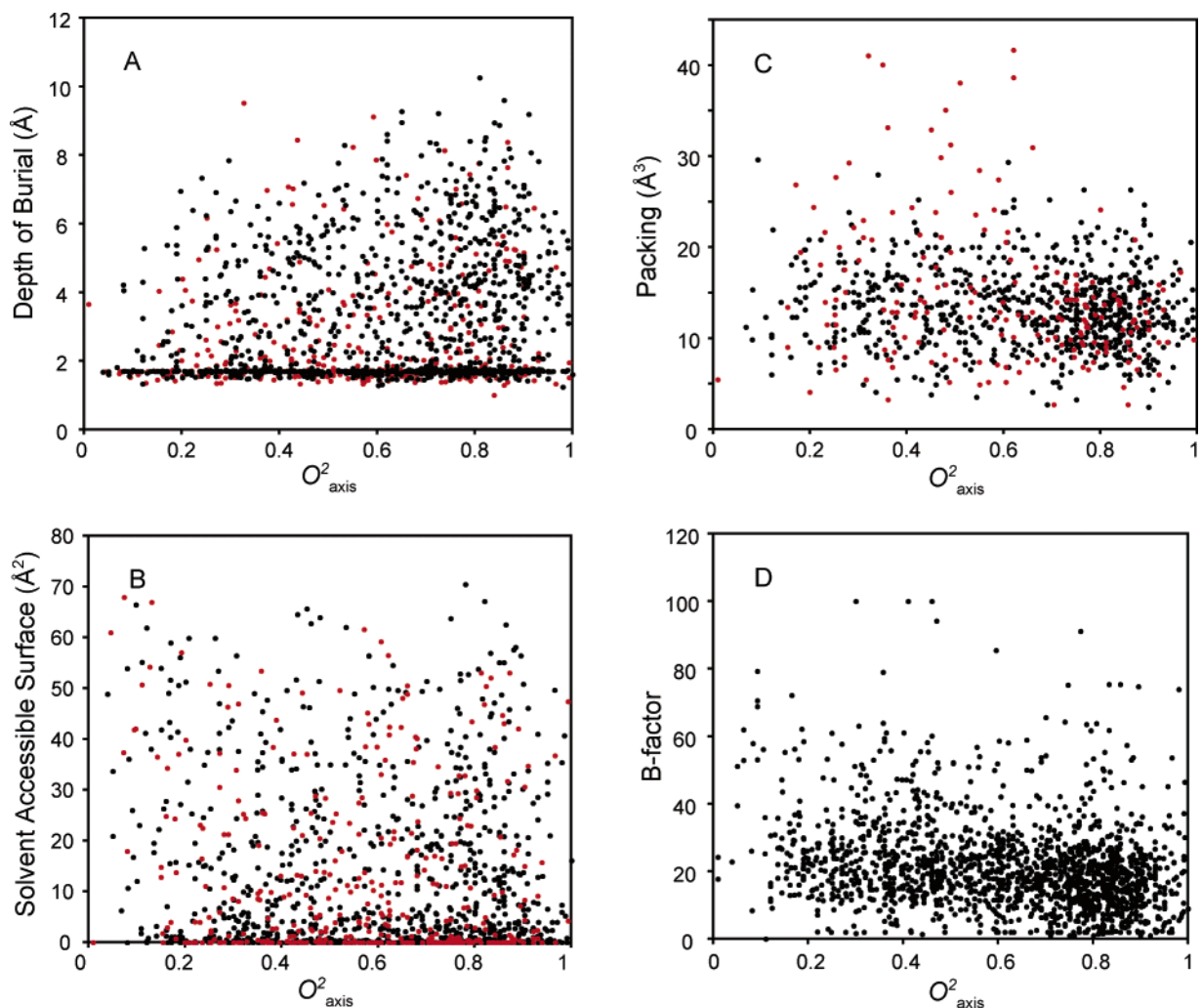
Figure 3. Correlation of experimentally determined methyl group dynamics with several primitive structural parameters. Methyl group symmetry axis squared generalized order parameters (O^2_{axis}) determined by deuterium relaxation were obtained from the literature (Table 2). Structural parameters were obtained from structural models determined by crystallography (black symbols) or by NMR spectroscopy (red symbols). Panel A: Correlation of O^2_{axis} with depth of burial. Depth of burial was calculated by determination of the shortest distance between the methyl carbon and a molecular surface created with a rolling sphere (1.4 Å radius) utilizing the GRASP program.[140] Panel B: Correlation of O^2_{axis} with solvent accessible surface area. The solvent accessible surface area was determined using a rolling sphere with a radius of 1.4 Å. Panel C: Correlation of O^2_{axis} with packing density as determined by subtraction of the van der Waals volume of the methyl group from the volume of the Vonoroi polyhedral. Packing density was determined only for buried sites (i.e. atoms with completed Vonoroi polyhedra). Panel D: Correlation of O^2_{axis} with crystallographic B-factors. In no case does the R^2 of the best fitted line to any of these data sets exceed 0.05.

dynamics.[95] The relative populations of these classes can vary significantly (Figure 5).[99] For example, flavodoxin is almost entirely devoid of the low and intermediate order parameter classes[100] while the high order parameter class is absent in α_3D, a protein of *de novo* design (Figure 5).[101] Note also that the centers of the distributions vary slightly across the three proteins. The three classes of motion have also been seen in Ile residues of malate synthase G, the largest protein examined by deuterium relaxation methods.[49] Thus, proteins are generally capable of a significant range of motional distributions, which is the raw material necessary for many potential functional applications of protein motion.

The distinctive grouping of order parameters seen in the calmodulin complex is often obscured in other proteins,[102] potentially due to issues of the statistics of low numbers and/ or extensive overlap of order parameter classes. Nevertheless, the motional origin of these classes is clear. In the case of calmodulin, two fundamental types of motion occurring on the sub-nanosecond time scale are involved: motion within

a rotamer well and motion between rotamer wells of side chain torsion angles.[93] It has been shown that the class of motion centered on a squared generalized order parameter value of ~0.35 generally involves a contribution from rotameric interconversion on the nanosecond or faster time scale as it leads to a significant averaging of scalar coupling (J) constants.[93] Indeed, simple theoretical considerations insist that this must be the case (Figure 6).[93] More recent experimental results[103] and theoretical simulations[98,104] suggest this to be general. We term this group the "J-class". The distribution of motion at the other extreme is centered on a squared generalized order parameter of ~0.85, which represents highly restricted motion within a rotamer well and is reminiscent of the relative rigidity of the polypeptide backbone. We term this class the "ω-class". The class of motion centered on a squared generalized order parameter of ~0.6 involves little detectable rotamer interconversion and therefore reflects both variation of the amplitude of motion within a single rotamer well and/or the superposition of
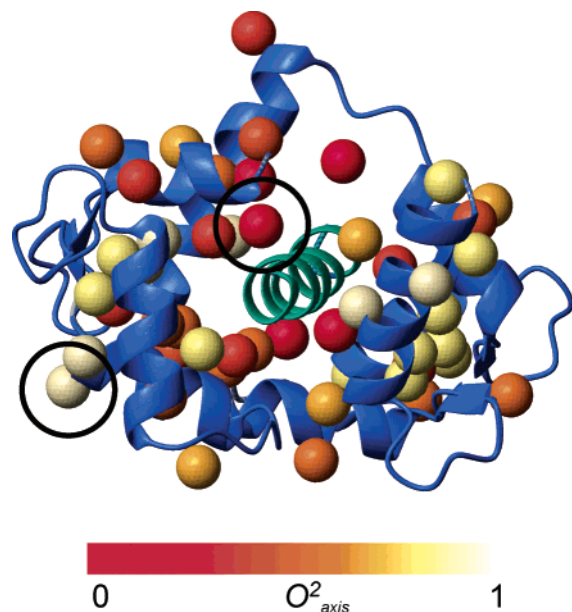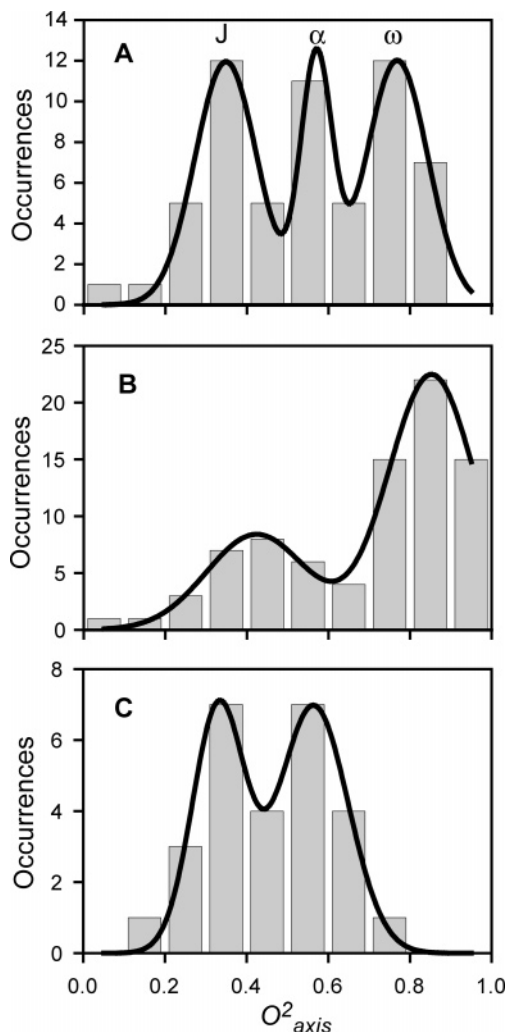
Figure 4. Distribution of amplitude of fast motion of methyl groups in a calmodulin/peptide complex. Shown is a ribbon representation of the backbone of the crystal structure (1CDL)[141] of the complex between calcium-saturated calmodulin and a peptide representing the calmodulin binding domain of the smooth muscle myosin light chain kinase. Methyl groups are represented by spheres that are color-coded according to their O^2_{axis} parameter determined by deuterium relaxation.[106] Note the circled methyl groups illustrating that being on the surface of the protein does not necessarily result in extensive amplitude of motion nor does complete burial necessarily result in highly restricted motion.

Figure 5. Histograms of the distribution of squared generalized order parameters of methyl group symmetry axes (O^2_{axis}) in (A) the complex of calcium-saturated calmodulin and a peptide derived from the calmodulin binding domain of the smooth muscle myosin light chain kinase,[106] (B) flavodoxin,[100] and (C) α_3d, a protein of de novo design.[101] Lines are best fits to a sum of three Gaussians for part A, giving $R^2 = 0.989$, and to a sum of two Gaussains for parts B and C, giving $R^2 = 0.999$ and 0.986, respectively.

motion about connected torsion angles. The distribution within this class is generally expected to reflect variance of amplitude of motion within rotamer wells, and we, therefore, term this class the "α-class". The distribution of the J-, α-, and ω-classes in the calmodulin/smMLCKp complex is satisfactorily described by a sum of three Gaussians (Figure 5). Randomization tests[105] indicate that this distribution is statistically significant and more appropriate than a random distribution or one described by one or two Gaussians.

Figure 5 is simply a gross overview of the distribution of methyl dynamics in proteins. Such composite histograms do not reveal the contributions of the various types of methyl-bearing amino acid residues to the total distribution. Obviously, the longer the side chain, the greater the number of degrees of freedom and, in principle, the greater the potential for significant angular disorder. However, these degrees of freedom are not always sampled. For example, methionine methyl groups are among the most rigid and the most dynamic of the methyl-bearing amino acid residues in calmodulin.[106] The distribution of O^2_{axis} values, determined by deuterium relaxation, for Ala, Thr, Ile, Val, Leu, and Met residues in proteins is shown in Figure 7. Clearly, the longer the side chain, the more degrees of freedom and the less predictable the dynamics of an attached methyl group. Though there has been at least one significant advance toward predicting the degree of motional disorder at methyl sites,[107] a truly quantitative understanding remains to be formulated.

## 5.3. Temperature Dependence

The absence of obvious structural and stereochemical determinants of the rich dynamical behavior seen in proteins is puzzling. The relationships between structure and dynamics

could potentially be illuminated by the temperature dependence of the dynamics. Variation of temperature provides access to the energetics of the motional modes contributing to the NMR relaxation phenomena. To date there has only been one comprehensive study of the temperature dependence of the fast methyl-bearing side chain dynamics of a protein. Lee and co-workers[93,95] examined the temperature dependence of the main chain and methyl-bearing side chain dynamics of calcium-saturated calmodulin (CaM) in complex with a peptide model for the smooth muscle myosin light chain kinase calmodulin binding domain (smMLCKp).[95] A significant temperature range was examined (15−73 °C). A synoptic analysis emphasizes the aforementioned trimodal distribution of angular disorder in calmodulin and appears to provide a simple explanation for the so-called glass transition observed in proteins at 200 K.[95] The temperature profiles of methyl O^2_{axis} parameters exhibit substantial variability in both absolute value and variation with temperature (Figure 8). On average, the temperature derivative of the O^2_{axis} parameter, σ, varies significantly for the different methyl types.[93] A number of the alanine methyl groups
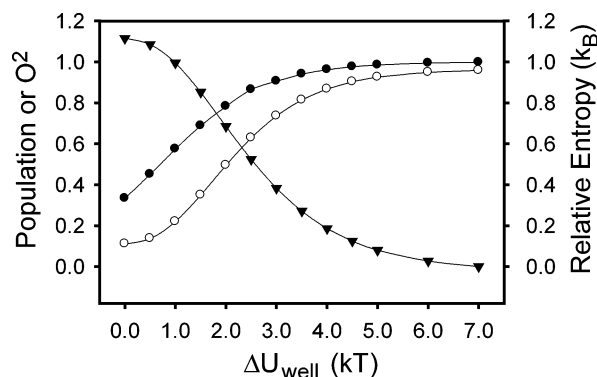
Figure 6. Dependence of the squared generalized order parameter and entropy on rotamer averaging. The curves were constructed using the potential energy function $U(\theta) = b_0 + b_1 \cos(\theta) + b_2 \cos(3\theta)$. The constant b_1 was set to $8kT$. The constant $b_2 = \Delta U_{well}/1.5$, and $b_0 = b_1 + b_2$. ΔU_{well} was varied from 0 to $8kT$ in steps of $0.5kT$. This function defines three wells, two of which are degenerate. ΔU_{well} defines the energy gap between the two degenerate wells and the third well. The lowermost curve corresponds to ΔU_{well} of zero. Shown is the fractional occupancy of the major rotamer (●), the value of O^2 (○), and the difference in entropy from the high ΔU_{well} limit (▼). Reproduced with permission from ref 93. Copyright 2002 American Chemical Society.
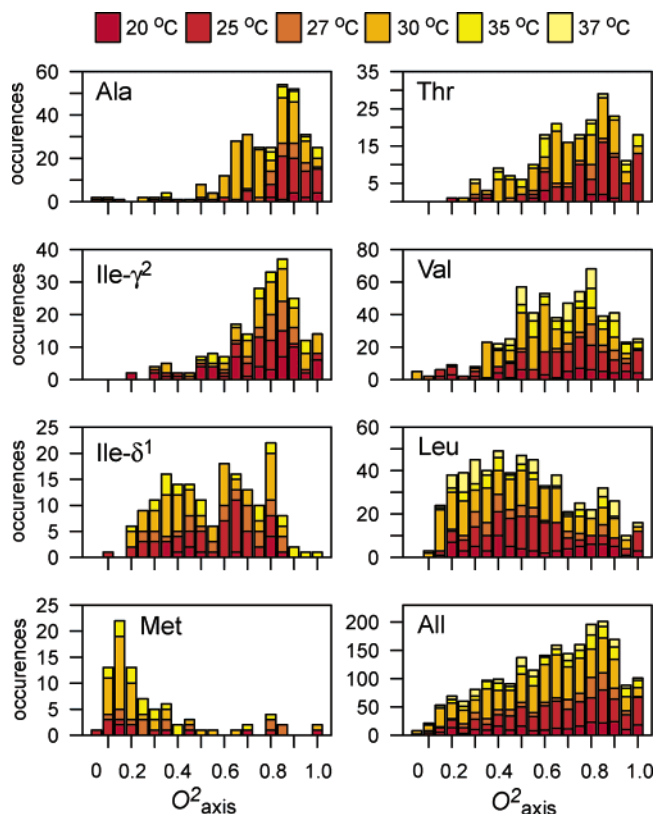
Figure 7. Histograms of the distribution of squared generalized order parameters of methyl group symmetry axes (O^2_{axis}) of the five types of methyl-bearing amino acid side chains in proteins. The O^2_{axis} values reported in the literature as summarized in Table 2 have been used. Because methyl group dynamics have a significant temperature dependence, O^2_{axis} parameters are identified with the temperature at which they were determined. In general, short chains tend to be more motionally restricted whereas longer side chains tend to have higher amplitudes of motion.

display an apparent increase in the amplitude of their dynamics as the temperature falls below 28 °C (Figure 8). This is unexpected. Above 28 °C, the thermal response is

Table 3. Thermal Coefficients of the Amplitude of Main Chain and Methyl-Bearing Side Chain Dynamics of Calcium-Saturated Calmodulin in Complex with the SmMLCKp Domain[a]

	no.[b]	σ ($\times 10^3$ K^{-1})	r^2
amide N−H (O^2_{NH})[c]	83	-1.5 ± 0.9	-0.89 ± 0.01
alanine βCH$_3$ (O^2_{axis})[d]	9	-1.2 ± 1.2	-0.57 ± 0.40
	9	-1.7 ± 0.1	-0.66 ± 0.29[e]
threonine γCH$_3$ (O^2_{axis})[d]	7	-3.9 ± 1.1	-0.97 ± 0.01
valine γCH$_3$ (O^2_{axis})[d]	10	-1.8 ± 1.7	-0.47 ± 0.73
isoleucine γCH$_3$ (O^2_{axis})[d]	6	-2.4 ± 0.9	-0.82 ± 0.24
isoleucine δCH$_3$ (O^2_{axis})[d]	8	-2.4 ± 1.2	-0.87 ± 0.19
leucine δCH$_3$ (O^2_{axis})[d]	7	-3.3 ± 1.3	-0.91 ± 0.07
methionine εCH$_3$ (O^2_{axis})[d]	7	-3.8 ± 2.0	-0.97 ± 0.02

[a] Temperature coefficients dO^2/dT or σ for the indicated group are derived from linear regression of all data available, except as noted. The Pearson coefficient of correlation (r^2) and its standard deviation are shown to describe the degree of linearity of the response to temperature. Taken from Lee et al.[93] [b] Number of sites for which reliable data at a minimum of three temperatures was available. [c] Excluding the 73 °C data set; see Lee et al.[93] [d] Excluding the 15 and 73 °C data sets; see Lee et al.[93] [e] Excluding the 15, 20, and 73 °C data sets; see Lee et al.[93]

roughly linear, having an average σ of $\sim -1.8 \times 10^{-3}$ K^{-1}, similar to the case of the backbone. It is interesting that the number of bonds by which methyl group is removed from the backbone does not necessarily dictate the corresponding dO^2_{axis}/dT. For example, valine methyls have a relatively flat response to temperature with an average σ of $\sim -1.8 \times 10^{-3}$ K^{-1}. Furthermore, isoleucine γ and δ methyls have equivalent average thermal coefficients. Threonines have the largest σ of $\sim -3.9 \times 10^{-3}$ K^{-1}, although this may be a result of most of the threonines having high solvent accessibility in this protein complex. Methionines have the most variable and, interestingly, the most linear response to changes in temperature (Figure 8). The amplitudes of motion of some methionine methyl groups are relatively temperature insensitive (e.g. Met-76, $\sigma \sim -1.1 \times 10^{-3}$ K^{-1}) while others have among the largest thermal coefficients in the protein (e.g. Met-71, $\sigma \sim -6.3 \times 10^{-3}$ K^{-1}). In this vein, there would appear to be a rough correlation between the linearity of the temperature dependence of the amplitude of the dynamics of a given amino acid side chain type, in the 28−67 °C range, and the number of bonds by which the methyl group is removed from the backbone (Table 3).

In an attempt to provide physical insight into the temperature dependence of the methyl-bearing side chain in the CaM/smMKLCKp complex, Lee and co-workers evaluated the generalized order parameters arising from motion in several simple azimuthally symmetric potential well models where the energy depends only on the angle θ with respect to the symmetry axis.[93]

The potentials considered were an infinite square well (SQ) of width θ_c; quadratic (U2), quartic (U4), and sixth power (U6) square wells; and a stepped square well (ST) where $U = 0$ for $\theta < \theta_s$ and $U = U_s$ for $\theta > \theta_s$ elsewhere. The power law and square well potentials are described by a single parameter, the force constant K or the well width, respectively. The square well potential would correspond to the often-used "free diffusion in a cone" model. The step potential has two parameters, the well width and the step height, θ_s and U_s, respectively. As anticipated, all of these potentials give a roughly linear temperature dependence for the corresponding squared generalized order parameter with the square well potential being temperature-independent and
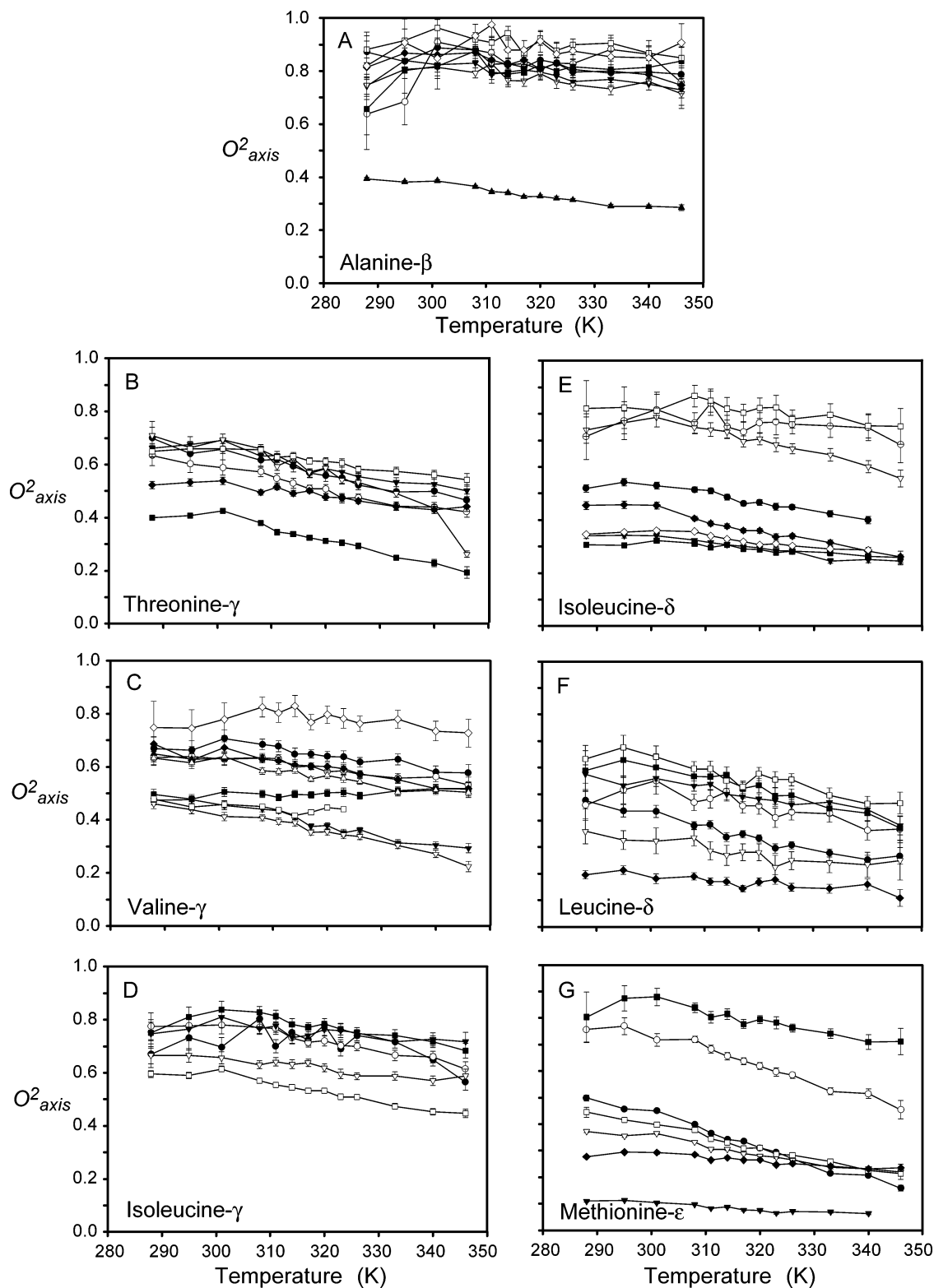
Figure 8. Temperature dependence of side chain methyl O^2_{axis} parameters of calmodulin in complex with the smMLCKp peptide. (A) Methyl O^2_{axis} parameters determined for the β methyl groups of alanines: A10 (●), A15 (○), A46 (▼), A73 (▽), A88 (■), A102 (□), A103 (◆), A128 (◇), and A147 (▲). (B) Methyl O^2_{axis} parameters determined for the γ methyl groups of threonines: T26 (●), T29 (○), T34 (▼), T70 (▽), T79 (■), T110 (□), and T146 (◆). (C) Methyl O^2_{axis} parameters determined for the γ methyl groups of valines: V35-γR (●), V35-γS (○), V55-γR (▼), V55-γS (▽), V108-γR (■), V108-γS (□), V121-γR (◆), V136-γR (◇), V142-γR (▲), and V142-γS. (D) Methyl O^2_{axis} parameters determined for isoleucine-γ methyls: I27 (●), I52 (○), I63 (▼), I85 (▽), I125 (■), and I130 (□). (E) Methyl O^2_{axis} parameters determined for isoleucine-δ methyls: I9 (●), I27 (○), I52 (▼), I63 (▽), I85 (■), I100 (□), I125 (◆), and I130 (◇). (F) Methyl O^2_{axis} parameters determined for leucine-δ methyls: L18δS (●), L39δR (○), L39δS (▼), L69δR (▽), L105δR (■), L112δS (□), and L116δR (◆). (G) Methyl O^2_{axis} parameters determined for methionine-ε methyls: M71 (●), M72 (○), M76 (▼), M109 (▽), M124 (■), M144 (□), and M145 (◆). In many cases the error bars are less than the dimensions of the symbol. Reproduced with permission from ref 93. Copyright 2002 American Chemical Society.
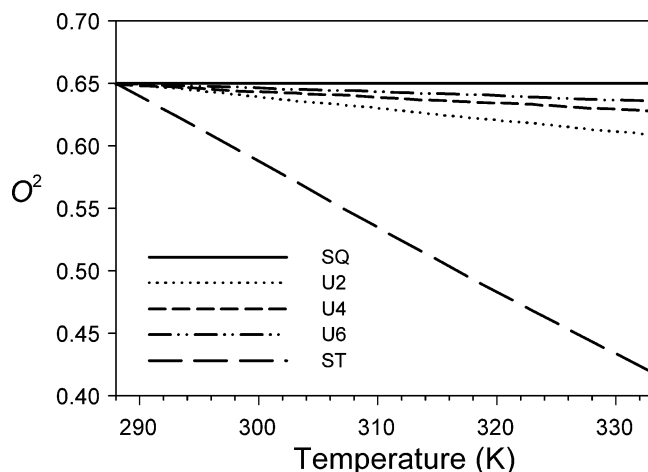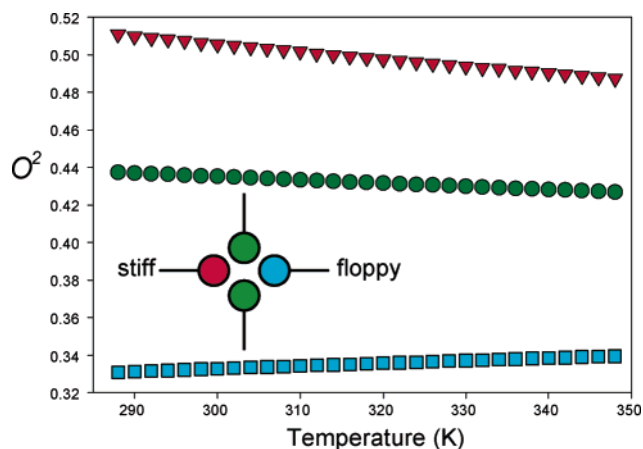
Figure 9. Temperature dependence of the O^2 parameter for a site moving in an infinite square well (SQ) potential or a quadratic (U2), quartic (U4), sixth-power (U6), or stepped square well (ST) potential. The models have been parametrized to give a O^2 parameter value of 0.65 at a temperature of 15 °C. Reproduced with permission from ref 93. Copyright 2002 American Chemical Society.

Figure 10. Temperature dependence of O^2 parameters of sites attached to four interacting side chains in a two-dimensional cluster model (inset). The green side chains have the same temperature dependence (●), the stiff red side chain (▼) and floppy blue side chain (■) have negative and positive temperature dependencies, respectively. Adapted with permission from ref 93. Copyright 2002 American Chemical Society.

the most anharmonic step potential being the most temperature sensitive (Figure 9). These simple physical models for the dependence of O^2 on temperature seem to show that no simple "effective potential" is sufficient to explain the high temperature dependence or to capture the rich variety of observed $O^2_{\text{axis}}(T)$'s. Even though the step-function potential has a relatively steep temperature dependence, it is, as are all of the simple models, essentially linear and fails to show sharp transitions or reversals in sign such as illustrated by Figure 8. Furthermore, Palmer and co-workers have elegantly shown that the simple harmonic (quadratic) potential has a theoretical upper limit for the temperature dependence of the generalized order parameter:[108]

$$\Lambda = \frac{d \ln(1 - O)}{d \ln T} \leq 1 \qquad (52)$$

Even for well-behaved sites (i.e. those having a linear temperature dependence), the methyl group O^2_{axis} parameters in the calmodulin complex exceed this upper limit by a factor of 3 or more.[93,95] Clearly, the simple azimuthally symmetric potentials fail to capture the quantitative aspects of the observed temperature dependence.

The failure of these simple models of motion in isolation is not too surprising since methyl groups are (usually) tightly packed in the protein, and have covalent and steric interactions with neighboring groups which are themselves moving, presumably in a highly coupled way. Thus, the potential seen by a group is itself a dynamically changing factor. The implications of these conceptually intuitive features can be represented in a simple two-dimensional cluster model, and the dynamic effects of steric conflict can be easily explored (Figure 10).[93] This model is characterized by four intrinsic potential step barriers, U_{s_i}, and four pairs of steric interaction parameters, $U_{ij}-\theta_{ij}$. Physically, the model can be thought of as describing the restricted range of angular motions intrinsic to each side chain because of covalent and backbone interactions, plus interactions with neighboring side chains, where larger values of U_{s_i}, U_{ij}, and θ_{ij} correspond to a stiffer side chain, a harder neighbor interaction, and a looser packing with the neighbor, respectively. Most of the potential

combinations examined gave monotonic, almost linear, decreasing O^2 with increasing temperature, with the expected variation among side chains, i.e., a higher O^2 for a stiffer side chain, for example. Some, however, mirror the unusual temperature dependence observed experimentally. For example, a scenario corresponding to a more heterogeneous cluster interaction gave a more interesting result (Figure 10). In that case, the dynamics of one stiff side chain ($U_{s_i} = 1$ kcal) having loose neighbor interactions ($U_{ij} = 5$ kcal, $\theta_{ij} = 0$) with three floppy side chains ($U_{s_i} = 0$) and making tight interactions with each of the others ($U_{ij} = 5$ kcal, $\theta_{ij} = 20$) were modeled. The central floppy blue side chain shows an increase in O^2 with increasing T, while the stiff red side chain shows a decrease in O^2, and the intervening green side chains show almost no temperature dependence. The perhaps surprising increase in O^2 can be rationalized in physical terms as follows. Each side chain is constrained to move in some "configurationally averaged" space provided by its two neighbors. The side chain itself will tend to explore a larger volume, as the temperature is increased. However, the "dynamic volume" occupied by its neighbors will also tend to increase as their excursions increase, sterically constraining the side chain. The net effect on the order parameter results from the competition between these two effects. In most scenarios, the first factor wins out, with the concomitant decrease in order parameter, since many of the large excursions made by the neighbors are in a direction away from the side chain. Neighboring side chain motions tend to be positively correlated by their steric interaction. However, the "dynamic volume" available to the central floppy neighbor in Figure 10 is gradually decreased at higher temperatures because the stiff side chain opposite it starts to undergo larger excursions, "pushing" on the floppy intervening green groups. This results in the increase in O^2 with temperature. In more formal terms, there is a negative angular correlation introduced between the motion of the red and blue side chains.[93] This result provides a simple and highly possible mechanism for long-range transmission of dynamic disorder in proteins. Finally, it was found that the entropy of this cluster model is ~60% of that of the four side chains moving independently within their individual energy potentials. This will be important in the consideration
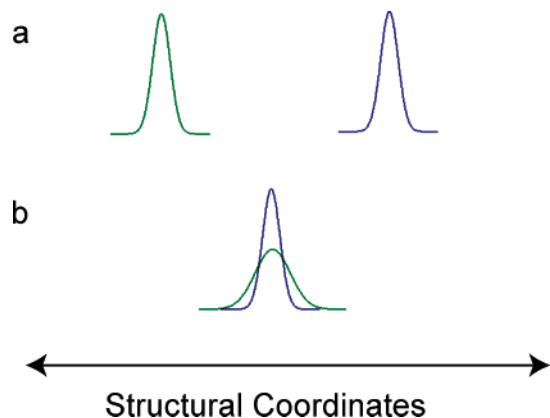
Figure 11. Simple schematic illustration of (a) allosteric mechanisms based solely on a change in atomic coordinates of the protein (b) and an allosteric mechanism based solely on entropic effects manifested in the dynamics of the protein. Structure-based allostery is the current paradigm, but as pointed out by Cooper and Dryden (1984), a change in conformational entropy also provides a plausible mechanism for creation of allosteric free energy changes in proteins. Only small changes in the breadth of the conformational distribution would be required if a large number of motional modes are involved. In principle, both mechanisms could be operative. Adapted by permission from Macmillan Publishers Ltd: *Nature Structural Biology* **2001**, *8*, 926−931 (http://nature.com/nsmb), ref 99. Copyright 2001.

of dynamics in terms of the conformational entropy that it represents (*vide infra*).

5.4. Functional Dynamics

5.4.1. Plausible Roles for Dynamics in Protein Function

In a provocative and inspiring paper, Dryden and Cooper examined the plausibility of Nature employing the residual entropy of proteins, manifested in their conformational dynamics, as a thermodynamic mechanism for allosteric responses to ligand binding.[109] The basic idea is illustrated and contrasted to the classical structural or mechanical enthalpic ("Rube Goldberg" view) mechanism in Figure 11. The potential for this kind of statistical thermodynamic linkage between conformational and binding equilibria is clear.[110,111] An entropically based allosteric mechanism could, in principle, be combined with the more classical mechanical or "enthalpic" view, where a discrete conformational change defines the allosteric transition. The central point is that if a large number of dynamical modes of the protein are involved in this sort of allosteric mechanism, then the change in conformational "breadth" (the width of the distributions shown in Figure 11) need only be on the order of a fraction of an Ångström to provide free energy changes ($\Delta\Delta G$) typical of allosteric activation. It is therefore not surprising that this sort of mechanism has not yet been revealed by structural methods such as X-ray crystallography. NMR relaxation appears to provide the best hope for detecting such allosteric mechanisms in proteins.

5.4.2. Prerequisites for Functionally Relevant Dynamics

In order for protein dynamics, and the entropy that it represents, to be involved in allosteric regulation, the dynamics of proteins needs to be significant, heterogeneously distributed, and malleable. The initial view of how significantly the internal dynamics of proteins could be perturbed by the binding of ligands came from the calmodulin system. Nitrogen-15 and deuterium relaxation methods were used

to examine the response of the picosecond to nanosecond dynamics of the main chain and of methyl-bearing side chains of calcium-saturated calmodulin (CaM) to the formation of a complex with a peptide model of the calmodulin binding domain of the smooth muscle myosin light chain kinase (smMLCKp).[106] The goal was to trace the local changes in dynamics in calmodulin upon moving from its free calcium-activated state to the complex with the smMLCKp domain. The O^2 values of methyl group symmetry axes (O^2_{axis}) of free CaM range from ∼1 to as low as ∼0.2. The lower values are, on average, significantly lower than those found for other proteins, especially for leucine and isoleucine methyl groups. Evidently, calcium-saturated calmodulin is an uncommonly dynamic protein on the picosecond to nanosecond time scale at the side chain level but not at the backbone level, as seen from ^{15}N relaxation. When complexed with the smMLCKp peptide, the order parameters of the side chain methyl groups are, on average, higher than those for unbound CaM, reflecting an overall loss of mobility upon binding the smMLCKp domain. Nevertheless, despite significant rigidification upon complexation, the O^2_{axis} values of methyl-bearing amino acids of calmodulin indicate the presence of considerable residual motion in the complex.

A difference plot illustrates the changes in O^2_{axis} values brought about by formation of the complex (Figure 12). On average, the O^2_{axis} parameters increase by 0.07 upon formation of the complex. The dynamic response to the binding of smMLCKp is nevertheless a mixed one, varying from decreases in O^2_{axis} for a few valine and leucine methyls to large increases in several methionine methyls. The significant reorganization of side chain dynamics that accompanies binding contrasts with the flat backbone response as observed by ^{15}N relaxation (Figure 12). This is particularly noteworthy in light of the relatively small structural response of the individual domains of CaM to the smMLCKp domain. Clearly, it is the side chains that report on the protein's unique dynamic behavior in "structured" regions, whereas the backbone of CaM, in either functional state, displays the generic order parameters (∼0.9) seen in so many other systems.

Nine of the proteins studied in detail using deuterium relaxation methods have been characterized in two (or more) states (Table 2). All of the proteins involved show significant and heterogeneously distributed dynamics. The fast dynamics of many methyl-bearing side chains in most of these proteins are significantly perturbed as they move from one functional state to another. Four examples are illustrated in Figure 13. This, as prescribed above, is the raw material necessary for functional relevance.

5.4.3. Conformational Entropy

Implicit in molecular motion is a "counting of states", and with it comes the potential to gain access to the residual conformational entropy that it represents.[92,99,112] The current approaches to extracting thermodynamic information from the dynamics captured by NMR relaxation find their roots in the work of Palmer and co-workers.[90] There, the Gaussian axial fluctuation model[89] was employed to investigate free energy relationships with the dynamic response reported by NMR relaxation. Access to entropy is illuminated by an alternate definition of the Lipari−Szabo generalized order parameter that reveals the underlying dependence on the
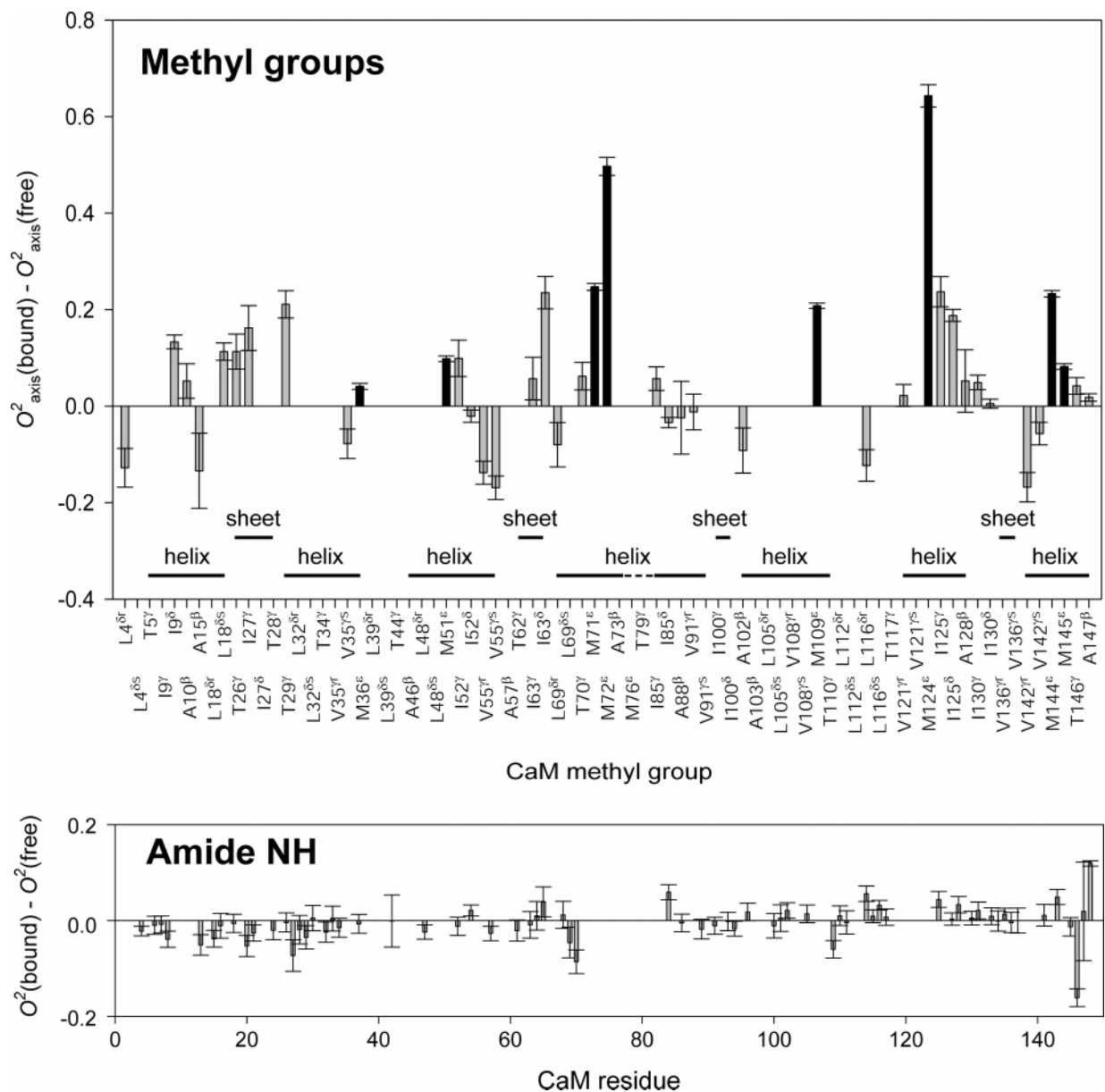
Figure 12. Response of the dynamics of calmodulin to binding of the smMLCKp domain. The top panel is for the side chain methyl groups, and the bottom panel is for the backbone NH groups. Secondary structure elements are indicated with solid lines. Methionines are highlighted in solid black. Adapted by permission from Macmillan Publishers Ltd: *Nature Structural Biology* **2000** 7, 72−77 (http://nature.com/nsmb), ref 106. Copyright 2000.

potential energy function governing the averaging described by eq 44 above. Here, the squared generalized order parameter is written as

$$O^2 = \sum_{m=-2}^{2} |\langle C_{2m}(\Omega) \rangle| =$$

$$\int\int p_{eq}(\Omega_1) \, P_2(\cos\theta_{12}) \, p_{eq}(\Omega_2) \, d\Omega_1 \, d\Omega_2 \quad (53)$$

The probability of a given orientation of the interaction vector of interest, $p_{eq}(\Omega)$, is defined by the potential energy function governing the system. This provides direct access to the partition function (Q) governing the system, as manifested in its fast internal dynamics, and hence illuminates the underlying thermodynamic parameters. By specifying the potential energy function, one is able to generate a model-specific parametric relationship between what can be measured, the generalized order parameter, and what is sought, the local residual entropy.[92]

A variety of models have been investigated in this context, including the simple infinite square well[91] and the harmonic oscillator.[92] In the context of entropy, the former gives a particularly simple parametric relationship between the experimentally accessible generalized order parameter and the corresponding absolute residual entropy:[91]

$$S = k_B \ln[\pi(3 - \sqrt{1 + 8O})] \quad (54)$$

Unfortunately, the more complicated models do not give unambiguous connections to *absolute* entropies. For example, the simple harmonic oscillator formally gives a family of functions relating the generalized order parameter to the corresponding entropy due to the essentially infinite range of possible parameters.[92] This ambiguity results in a family of lines such as that shown in Figure 1 of Li et al.[92] Fortunately, *differences* in entropy are much more reliably estimated if a few reasonable assumptions are made: that the nature of the motion does not change appreciably between
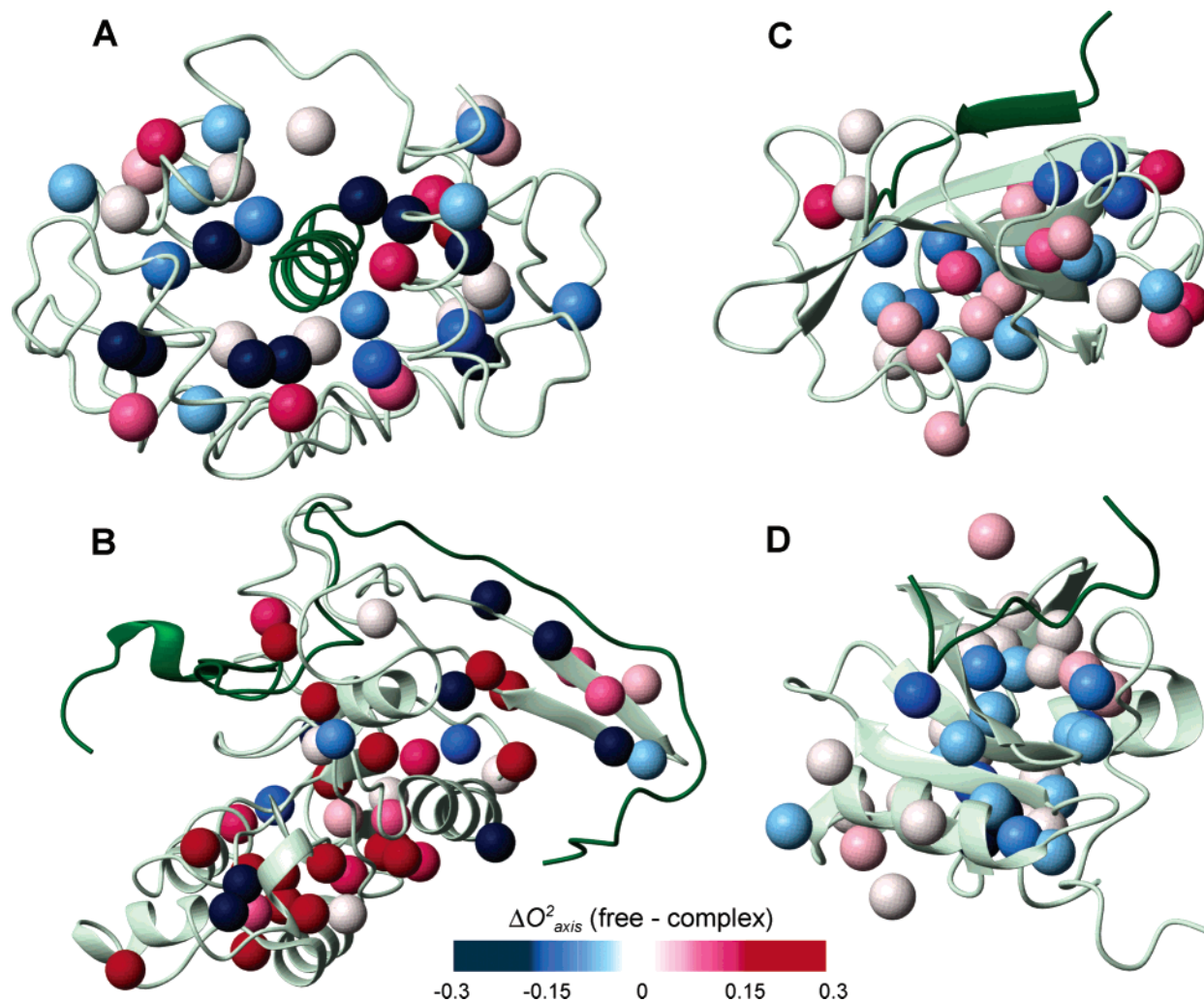
Figure 13. Examples of perturbation of methyl-bearing side chain dynamics due to the binding of ligands. Ligands are shown in dark green, protein backbones in white, and methyl carbons as balls that are colored to reflect the change in ΔO^2_{axis} parameter between the uncomplexed and complexed states. Blues represent sites that are more rigid in the complex, and reds are sites that are more mobile. (A) Calmodulin in complex with the smMLCK peptide (based on PDB code 1CDL). (B) PLCC SH2 in complex with the Y281 peptide (based on PDB code 1D4Z). (C) CdcHs42 in complex with PDB42 and GDPPCP (based on PDB code 1EES). (D) Phospholipase Cγ1 SH2 domain in complex with the pY1021 PDGFR peptide (based on PDB code 2PLE). Note the clustering of methyl groups near ligand binding sites that become more rigid upon binding and the propensity for methyl groups with increased amplitude of motion at solvent exposed sites distant from the ligand binding site. Prepared with MolMol.[142]

states, that the same oscillator is involved, and that correlated motion is limited.[92,93] For the simple models discussed here, the parametric relationship between the measurable generalized order parameter and the corresponding residual entropy is easily calculated (Figure 15).[92,93]

In this context, the results of Lee et al.[106] are particularly interesting when viewed from the point of view of the underlying thermodynamics of binding of target domains by calmodulin. Wintrode and Privalov[113] attempted to dissect the change in conformational entropy of calmodulin upon binding the smMLCKp domain from the system thermodynamic parameters obtained from calorimetric measurements. As they point out, this required a significant number of assumptions and speculations about the change in entropy of water and of the peptide upon formation of the complex. Wintrode and Privalov speculated that the change in the residual entropy of calmodulin could be up to −50 to −100 kcal/mol of entropy upon binding the domain.[113] Making the assumption that changes in the fast dynamics of methyl-bearing amino acids reflect the entire protein and that the simple harmonic motion model is applicable, Lee et al.

estimated that the change in dynamics was found to correspond to a change in conformational entropy of calmodulin on the order of −35 kcal/mol.[106] Obviously, there are difficulties with this crude interpretation (see above), but the sheer magnitude of the change is impressive and the fact that it is in line with the speculations of Wintrode and Privalov[113] is very encouraging. It is also interesting to note that even though many calmodulin binding domains associate with calmodulin with roughly the same affinity, the thermodynamic origins of the binding free energy can be quite different.[114] This raises the intriguing possibility that variation in the overall entropy of binding will be manifested in the dynamics of the protein.

5.4.4. Thermodynamic Particle versus Dynamic Pathways

Long-range "transmission" of perturbation of side chain dynamics correlated with a change in functional state has been clearly observed in several systems. An early and particularly interesting example is the study of three different functional states of Cdc42Hs, a member of the Ras superfamily of GTP binding proteins.[115] Members of this family
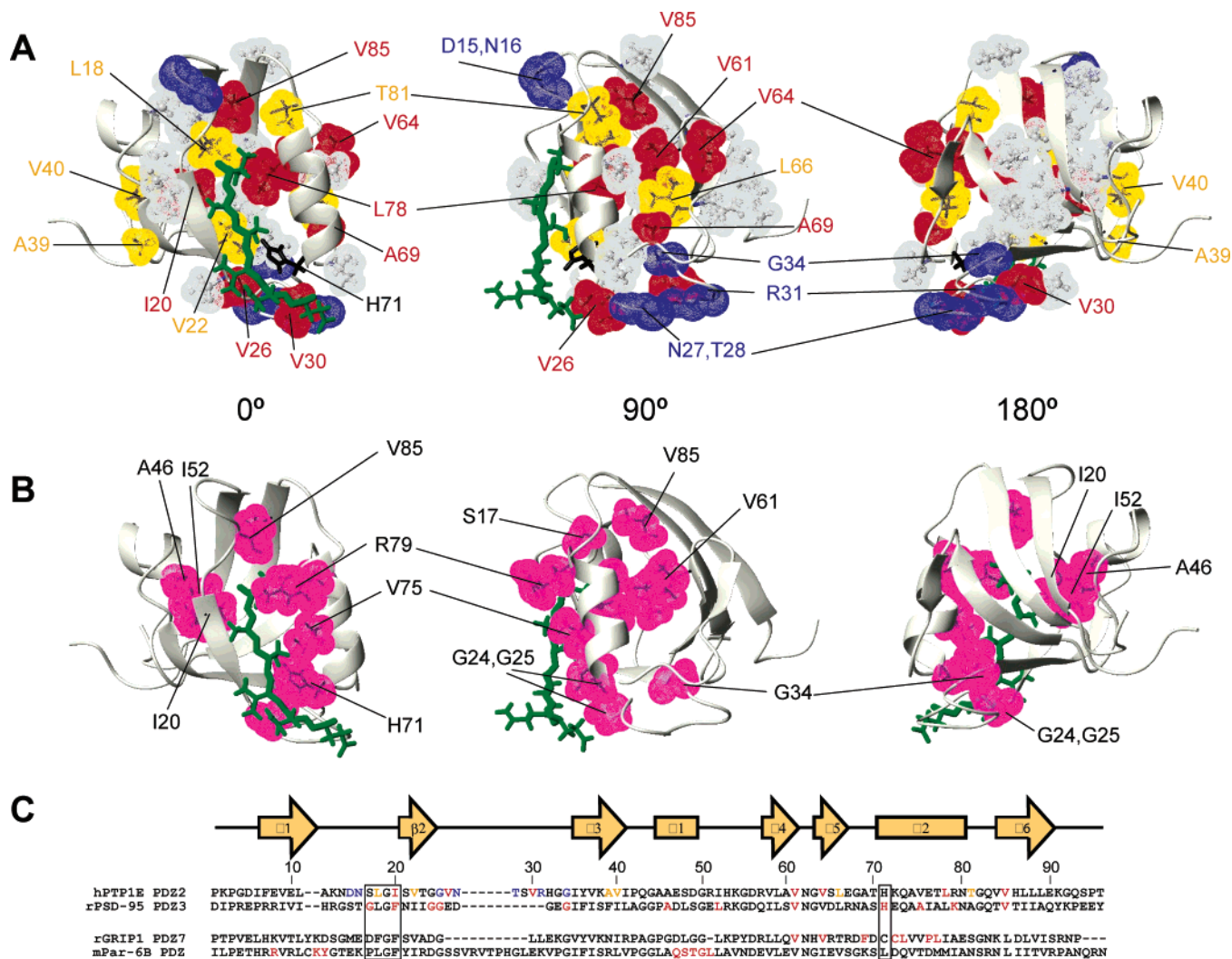
Figure 14. Comparison between dynamically linked residues in a PDZ domain and thermodynamic couplings predicted from a family of PDZ domains. (A) A summary of residues whose dynamical parameters change significantly upon peptide binding mapped onto the structure of the PDZ2/RA-GEF2 complex. The PDZ2 protein secondary structure is colored gray while the peptide ligand is green. Red VDW surfaces are side chain methyl residues that had appreciable ΔO^2_{axis}, in yellow are those methyl residues with appreciable $\Delta \tau_e$, and in blue are backbone NH groups that displayed changes in motion on the chemical shift time scale. Methyl groups not having changes in dynamics parameters are represented as gray VDW surfaces. Residues that were not compared are shown in black. For clarity, three views are presented. Residues of importance are labeled. (B) The statistical couplings derived from Lockless and Ranganathan[119] are mapped onto the PDZ1/RA-DEF2 structure shown in identical views as in part A. (C) Primary sequences of four PDZ domains color coded as in part A. See Fuentes et al.[122] for more detail. Reprinted from *Journal of Molecular Biology 335*, Fuentes, E. J., Der, C. J., Lee, A. L., Ligand-dependent dynamics and intramolecular signaling in a PDZ domain, pages 1105–15, Copyright 2004, with permission from Elsevier.

are activated by the exchange of GDP for GTP. Cdc42Hs interacts with a variety of proteins that serve to control the signal transduction. Loh et al. characterized the dynamics of backbone amide N–H's and side chain methyls of Cdc42Hs in complex with GDP, a GTP analogue and a domain derived from the p21-activated kinase effector of Cdc42Hs.[115] 15N-relaxation studies indicated that activation (replacement of GDP with a non-hydrolyzable analogue of GTP) has little effect on the dynamics of the backbone, while binding of the effector domain results in a significant decrease in the complexity of the backbone motion with the dynamics being shifted and confined to shorter time scales. Similarly, the activation of Cdc42Hs results in only small perturbations of the motion of methyl-bearing side chains in the protein. The binding of the effector domain, however, has a very intriguing effect—it causes a general *increase* in side chain mobility that is most pronounced for residues *remote* from the effector–Cdc42Hs interface. This presented the first clear evidence for the long-range transmission of

dynamic disorder on the sub-nanosecond time scale that was allosterically relevant.

The apparent participation of protein dynamics (entropy) in the thermodynamics of the binding of ligands, for example, need not have a coherent view when interpreted in the context of a single structure representing the native state.[116] This is certainly true for perturbations of fast internal dynamics where one does not often see spatially contiguous responses to binding events.[117] This would represent a simple thermodynamic particle view of the distribution of dynamic responses to changes in protein functional state where the principle result is to influence the thermodynamics governing biological function by modulation of the contribution of protein conformational entropy. This is perhaps the dominant role in the calmodulin system discussed above, though there are indeed hints that allosterically relevant dynamics do exist in that system.[117]

Perhaps implicit in the idea of transmission of dynamic disorder is the question of correlated motion. The answer
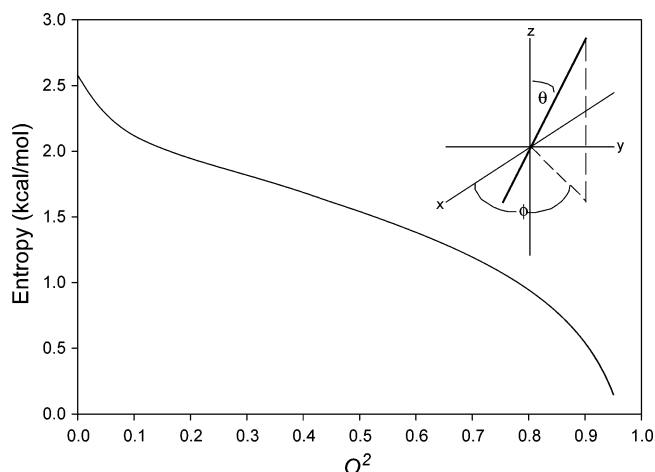
Figure 15. Parametric relationship between the generalized order parameter, reported by a nuclear interaction vector situated as a spy on an azimuthally symmetric harmonic oscillator, and the corresponding entropy.[92] Here a simple quadratic potential is used and a parametric relationship exists between the entropy of the oscillator (inset) and the O^2 parameter created by varying the force constant governing the potential energy. Uncertainty in the reduced mass, the depth of the energy well, and the effective length of the oscillator reduces the utility of the method for obtaining absolute entropies. However, estimates of differences in entropy are anticipated to be at least semiquantitative (see text).

may be highly context dependent. For example, using the small protein domain B1 from Streptococcal protein G, Stone and co-workers examined the methyl-bearing side chain dynamics of 10 mutants of varying stability.[118] A weak though statistically significant covariation of methyl group dynamics was observed, somewhat reducing the concern about the impact of correlated motion on the model-dependent interpretation of dynamical parameters. Nevertheless, the idea that proteins have *defined* pathways to transmit information (energy) in the native state—in this case in the form of increased/decreased motion—from one site to an allosteric site is still an intriguing possibility.

In this context, Lockless and Ranganathan have found statistical couplings between amino acids using multiple sequence alignments of hundreds of sequences of a protein domain.[119] They found that the evolutionarily conserved residues often form a continuous pathway of physical linkage though the protein and that mutation of statistically coupled pair residues affected ligand binding. There is mounting evidence that intramolecular, energetic networks in a wide variety of proteins are sparsely distributed throughout their structures.[120,121] For many proteins, the transmission of information occurs in the absence of large structural rearrangements, suggesting another role for side chain dynamics. Perhaps the most elegant experimental case for the dynamics-mediated transmission of allosteric signals is that made by Lee and co-workers for the PDZ domain (Figure 14).[122] They directly detect allosteric behavior using side chain methyl dynamics measurements. The changes in side chain dynamics parameters for a PDZ domain were determined upon binding a peptide target. Long-range dynamic effects were detected that correspond to previously observed statistical energetic couplings,[119] providing one of the first experimental examples for the potential role of picosecond to nanosecond time scale dynamics in propagating long-range signals within a protein, and reinforcing the idea that dynamic fluctuations in proteins can contribute to allosteric signal transduction. The fact that the few cases characterized thus far give such a range of insights propels further investigation.

6. Summary and Future Directions

We have tried to provide a compact summary of the current state-of-the-art of solution NMR-based characterization of the fast internal dynamics of protein side chains. The general effort has come a long way over the past decade with new and more powerful experiments being introduced and allowing for the comprehensive examination of side chain dynamics in over two dozen systems of significant size. The initial insights are puzzling in many respects and go against much of what is intuitively expected. The amplitudes of side chain dynamics are quite variable and heterogeneously distributed throughout the protein molecule. Classes of motion in methyl-bearing side chains have been observed and are largely understood in terms of the degree of barrier crossing between rotamers. The fast dynamics of methyl-bearing side chains can be significantly perturbed upon a change in functional state, such as the binding of a ligand to the protein. The dynamical response can be local or transmitted across the protein to sites remote from the binding site. Apparent pathways of dynamical coupling have been observed in some cases but not all. These observations provide the fundamental material for a role of protein dynamics, and the entropy that it represents, in the thermodynamic control of protein-mediated processes.

Despite these great strides, much remains to be discovered. For example, the current view of side chain dynamics is "methyl-centric" with almost no information available on the fast motion of side chains lacking methyl groups. Additional experimental approaches are required to expose the dynamics at these sites. Finally, and perhaps somewhat ironically, most information about "functional motion" has focused on the thermodynamic aspects rather than the kinetic or dynamical aspects of protein function, i.e., catalysis. Intriguing insights into the potential role of fast protein motion in enzymatic processes have emerged in the context of NMR relaxation studies of nuclei on the main chain (see Jarymowycz and Stone's[7] review in this issue), but studies have not yet moved to the side chains using the methods described here. This is an area that is ripe for exploration.

7. Abbreviations

$\{^1H\}-^{13}C$ NOE	$^1H-^{13}C$ nuclear Overhauser effect
2D	two-dimensional
3D	three-dimensional
CPMG	Carr−Purcell−Meiboom−Gill
CSA	chemical shielding anisotropy
DQ	double quantum
GAF	Gaussian axial fluctuations
HMQC	heteronuclear multiple quantum coherence
HSQC	heteronuclear single quantum coherence
INEPT	insensitive nuclei enhanced by polarization transfer
O^2 and O^2_{axis}	Lipari−Szabo squared generalized order parameter
S	entropy
T_1 (R_1)	spin−lattice relaxation time (rate)
T_2 (R_2)	spin−spin relaxation time (rate)
$T_{1\rho}$ $(R_{1\rho})$	spin−lattice relaxation time (rate) in the rotating frame
τ_e	internal effective correlation time for the local motion
τ_m	correlation time for the overall isotropic rotational motion

TOCSY   total correlation spectroscopy
TROSY   transverse relaxation optimized spectroscopy
ZQ   zero quantum

8. Acknowledgments

9. References

(1) Englander, S. W.; Kallenbach, N. R. *Q. Rev. Biophys.* **1983**, *16*, 521.
(2) Weber, G. *Adv. Protein Chem.* **1975**, *29*, 1.
(3) Gurd, F. R.; Rothgeb, T. M. *Adv. Protein Chem.* **1979**, *33*, 73.
(4) Frauenfelder, H.; Parak, F.; Young, R. D. *Annu. Rev. Biophys. Biophys. Chem.* **1988**, *17*, 451.
(5) Frauenfelder, H.; Sligar, S. G.; Wolynes, P. G. *Science* **1991**, *254*, 1598.
(6) Onuchic, J. N.; Luthey-Schulten, Z.; Wolynes, P. G. *Annu. Rev. Phys. Chem.* **1997**, *48*, 545.
(7) Jarymowycz, V. A.; Stone, M. J. *Chem. Rev.* **2006**, *106*, http://dx.doi.org/10.1021/cr040421p.
(8) Tolman, J. R.; Ruan, K. *Chem. Rev.* **2006**, *106*, http://dx.doi.org/10.1021/cr040429z.
(9) Palmer, A. G., III; Massi, F. *Chem. Rev.* **2006**, *106*, http://dx.doi.org/10.1021/cr0404287.
(10) Sattler, M.; Schleucher, J.; Griesinger, C. *Prog. Nucl. Magn. Reson. Spectrosc.* **1999**, *34*, 93.
(11) Kay, L. E. *J. Magn. Reson.* **2005**, *173*, 193.
(12) McIntosh, L. P.; Dahlquist, F. W. *Q. Rev. Biophys.* **1990**, *23*, 1.
(13) LeMaster, D. M. *Prog. Nucl. Magn. Reson. Spectrosc.* **1994**, *26*, 371.
(14) Kay, L. E.; Torchia, D. A.; Bax, A. *Biochemistry* **1989**, *28*, 8972.
(15) Wand, A. J.; Bieber, R. J.; Urbauer, J. L.; McEvoy, R. P.; Gan, Z. H. *J. Magn. Reson., Ser. B* **1995**, *108*, 173.
(16) Muhandiram, D. R.; Yamazaki, T.; Sykes, B. D.; Kay, L. E. *J. Am. Chem. Soc.* **1995**, *117*, 11536.
(17) Abragam, A. *Principles of nuclear magnetism*; Clarendon Press: Oxford, 1961.
(18) Hoffman, R. A. *Adv. Magn. Reson.* **1970**, *4*, 88.
(19) Cavanagh, J.; Fairbrother, W. J.; Palmer, A. G.; Skelton, N. J. *Protein NMR Spectroscopy: Principles and Practice*; Academic Press: San Diego, 1996.
(20) Fischer, M. W. F.; Majumdar, A.; Zuiderweg, E. R. P. *Prog. Nucl. Magn. Reson. Spectrosc.* **1998**, *33*, 207.
(21) Luginbuhl, P.; Wüthrich, K. *Prog. Nucl. Magn. Reson. Spectrosc.* **2002**, *40*, 199.
(22) Jacobsen, J. P.; Bildsoe, H. K.; Schaumburg, K. *J. Magn. Reson.* **1976**, *23*, 153.
(23) Millet, O.; Muhandiram, D. R.; Skrynnikov, N. R.; Kay, L. E. *J. Am. Chem. Soc.* **2002**, *124*, 6439.
(24) Skrynnikov, N. R.; Millet, O.; Kay, L. E. *J. Am. Chem. Soc.* **2002**, *124*, 6449.
(25) Yang, D. W.; Mittermaier, A.; Mok, Y. K.; Kay, L. E. *J. Mol. Biol.* **1998**, *276*, 939.
(26) Ernst, M.; Ernst, R. R. *J. Magn. Reson., Ser. A* **1994**, *110*, 202.
(27) Idiyatullin, D.; Daragan, V. A.; Mayo, K. H. *J. Magn. Reson.* **2004**, *171*, 4.
(28) Kay, L. E.; Torchia, D. A. *J. Magn. Reson.* **1991**, *95*, 536.
(29) Daragan, V. A.; Mayo, K. H. *J. Magn. Reson., Ser. B* **1995**, *107*, 274.
(30) Goto, N. K.; Kay, L. E. *Curr. Opin. Struct. Biol.* **2000**, *10*, 585.
(31) Tugarinov, V.; Kay, L. E. *ChemBioChem* **2005**, *6*, 1567.
(32) Henry, G. D.; Weiner, J. H.; Sykes, B. D. *Biochemistry* **1986**, *25*, 590.
(33) Nicholson, L. K.; Kay, L. E.; Baldisseri, D. M.; Arango, J.; Young, P. E.; Bax, A.; Torchia, D. A. *Biochemistry* **1992**, *31*, 5253.
(34) Palmer, A. G.; Rance, M.; Wright, P. E. *J. Am. Chem. Soc.* **1991**, *113*, 4371.
(35) Wand, A. J.; Urbauer, J. L.; McEvoy, R. P.; Bieber, R. J. *Biochemistry* **1996**, *35*, 6116.
(36) Lee, A. L.; Urbauer, J. L.; Wand, A. J. *J. Biomol. NMR* **1997**, *9*, 437.
(37) Rosen, M. K.; Gardner, K. H.; Willis, R. C.; Parris, W. E.; Pawson, T.; Kay, L. E. *J. Mol. Biol.* **1996**, *263*, 627.
(38) LeMaster, D. M.; Kushlan, D. M. *J. Am. Chem. Soc.* **1996**, *118*, 9255.
(39) Ishima, R.; Louis, J. M.; Torchia, D. A. *J. Biomol. NMR* **2001**, *21*, 167.
(40) Gardner, K. H.; Kay, L. E. *J. Am. Chem. Soc.* **1997**, *119*, 7599.
(41) Chaykovski, M. M.; Bae, L. C.; Cheng, M. C.; Murray, J. H.; Tortolani, K. E.; Zhang, R.; Seshadri, K.; Findlay, J.; Hsieh, S. Y.; Kalverda, A. P.; Homans, S. W.; Brown, J. M. *J. Am. Chem. Soc.* **2003**, *125*, 15767.
(42) Teilum, K.; Brath, U.; Lundstrom, P.; Akke, M. *J. Am. Chem. Soc.* **2006**, *128*, 2506.
(43) Ollerenshaw, J. E.; Tugarinov, V.; Skrynnikov, N. R.; Kay, L. E. *J. Biomol. NMR* **2005**, *33*, 25.
(44) Torizawa, T.; Shimizu, M.; Taoka, M.; Miyano, H.; Kainosho, M. *J. Biomol. NMR* **2004**, *30*, 311.
(45) Torizawa, T.; Terauchi, T.; Ono, A.; Kainosho, M. *Tanpakushitsu Kakusan Koso* **2005**, *50*, 1375.
(46) Kainosho, M.; Torizawa, T.; Iwashita, Y.; Terauchi, T.; Mei Ono, A.; Guntert, P. *Nature* **2006**, *440*, 52.
(47) Kay, L. E.; Bull, T. E.; Nicholson, L. K.; Griesinger, C.; Schwalbe, H.; Bax, A.; Torchia, D. A. *J. Magn. Reson.* **1992**, *100*, 538.
(48) Yang, D. W.; Kay, L. E. *J. Magn. Reson., Ser. B* **1996**, *110*, 213.
(49) Tugarinov, V.; Ollerenshaw, J. E.; Kay, L. E. *J. Am. Chem. Soc.* **2005**, *127*, 8214.
(50) Lee, A. L.; Flynn, P. F.; Wand, A. J. *J. Am. Chem. Soc.* **1999**, *121*, 2891.
(51) Ishima, R.; Petkova, A. P.; Louis, J. M.; Torchia, D. A. *J. Am. Chem. Soc.* **2001**, *123*, 6164.
(52) Tugarinov, V.; Kay, L. E. *Biochemistry* **2005**, *44*, 15970.
(53) Daragan, V. A.; Kloczewiak, M. A.; Mayo, K. H. *Biochemistry* **1993**, *32*, 10580.
(54) Zheng, Y.; Yang, D. W. *J. Biomol. NMR* **2004**, *28*, 103.
(55) Liu, W. D.; Zheng, Y.; Cistola, D. P.; Yang, D. W. *J. Biomol. NMR* **2003**, *27*, 351.
(56) Tugarinov, V.; Kay, L. E. *J. Biomol. NMR* **2004**, *29*, 369.
(57) Tugarinov, V.; Hwang, P. M.; Ollerenshaw, J. E.; Kay, L. E. *J. Am. Chem. Soc.* **2003**, *125*, 10420.
(58) Ollerenshaw, J. E.; Tugarinov, V.; Kay, L. E. *Magn. Reson. Chem.* **2003**, *41*, 843.
(59) Lipari, G.; Szabo, A. *J. Am. Chem. Soc.* **1982**, *104*, 4559.
(60) Lipari, G.; Szabo, A. *J. Am. Chem. Soc.* **1982**, *104*, 4546.
(61) Brink, D. M.; Satchler, G. R. *Angular Momentum*; Clarendon Press: Oxford, 1968.
(62) Vugmeyster, L.; Raleigh, D. P.; Palmer, A. G., 3rd; Vugmeister, B. E. *J. Am. Chem. Soc.* **2003**, *125*, 8400.
(63) Frauenfelder, H.; Wolynes, P. G. *Science* **1985**, *229*, 337.
(64) Wang, J.; Wolynes, P. *Chem. Phys. Lett.* **1993**, *212*, 427.
(65) Zhou, H. X.; Zwanzig, R. *J. Chem. Phys.* **1991**, *94*, 6147.
(66) Lee, A. L.; Wand, A. J. *J. Biomol. NMR* **1999**, *13*, 101.
(67) McMahon, M. T.; Oldfield, E. *J. Biomol. NMR* **1999**, *13*, 133.
(68) Henry, E. R.; Szabo, A. *J. Chem. Phys.* **1985**, *82*, 4753.
(69) Ottiger, M.; Bax, A. *J. Am. Chem. Soc.* **1998**, *120*, 12334.
(70) Woessner, D. E. *J. Chem. Phys.* **1962**, *37*, 647.
(71) Schurr, J. M.; Babcock, H. P.; Fujimoto, B. S. *J. Magn. Reson., Ser. B* **1994**, *105*, 211.
(72) Bruschweiler, R.; Liao, X. B.; Wright, P. E. *Science* **1995**, *268*, 886.
(73) Lee, L. K.; Rance, M.; Chazin, W. J.; Palmer, A. G. *J. Biomol. NMR* **1997**, *9*, 287.
(74) Zheng, Z. W.; Czaplicki, J.; Jardetzky, O. *Biochemistry* **1995**, *34*, 5212.
(75) Tjandra, N.; Feller, S. E.; Pastor, R. W.; Bax, A. *J. Am. Chem. Soc.* **1995**, *117*, 12562.
(76) Kneller, J. M.; Lu, M.; Bracken, C. *J. Am. Chem. Soc.* **2002**, *124*, 1852.
(77) Bruschweiler, R. *Curr. Opin. Struct. Biol.* **2003**, *13*, 175.
(78) Korzhnev, D. M.; Billeter, M.; Arseniev, A. S.; Orekhov, V. Y. *Prog. Nucl. Magn. Reson. Spectrosc.* **2001**, *38*, 197.
(79) Dellwo, M. J.; Wand, A. J. *J. Am. Chem. Soc.* **1989**, *111*, 4571.
(80) Chatfield, D. C.; Szabo, A.; Brooks, B. R. *J. Am. Chem. Soc.* **1998**, *120*, 5301.
(81) Schneider, D. M.; Dellwo, M. J.; Wand, A. J. *Biochemistry* **1992**, *31*, 3645.
(82) Clore, G. M.; Szabo, A.; Bax, A.; Kay, L. E.; Driscoll, P. C.; Gronenborn, A. M. *J. Am. Chem. Soc.* **1990**, *112*, 4989.
(83) Choy, W. Y.; Kay, L. E. *J. Biomol. NMR* **2003**, *25*, 325.
(84) Mandel, A. M.; Akke, M.; Palmer, A. G. *J. Mol. Biol.* **1995**, *246*, 144.
(85) d'Auvergne, E. J.; Gooley, P. R. *J. Biomol. NMR* **2003**, *25*, 25.
(86) Peng, J. W.; Wagner, G. *Biochemistry* **1992**, *31*, 8571.
(87) Peng, J. W.; Wagner, G. *J. Magn. Reson.* **1992**, *98*, 308.
(88) Daragan, V. A.; Mayo, K. H. *Prog. Nucl. Magn. Reson. Spectrosc.* **1997**, *31*, 63.
(89) Bruschweiler, R.; Wright, P. E. *J. Am. Chem. Soc.* **1994**, *116*, 8426.
(90) Akke, M.; Bruschweiler, R.; Palmer, A. G. *J. Am. Chem. Soc.* **1993**, *115*, 9832.
(91) Yang, D.; Kay, L. E. *J. Mol. Biol.* **1996**, *263*, 369.
(92) Li, Z.; Raychaudhuri, S.; Wand, A. J. *Protein Sci.* **1996**, *5*, 2647.

(93) Lee, A. L.; Sharp, K. A.; Kranz, J. K.; Song, X. J.; Wand, A. J. *Biochemistry* **2002**, *41*, 13814.

(94) Prompers, J. J.; Bruschweiler, R. *J. Phys. Chem. B* **2000**, *104*, 11416.

(95) Lee, A. L.; Wand, A. J. *Nature* **2001**, *411*, 501.

(96) Best, R. B.; Clarke, J.; Karplus, M. *J. Am. Chem. Soc.* **2004**, *126*, 7734.

(97) Prabhu, N. V.; Lee, A. L.; Wand, A. J.; Sharp, K. A. *Biochemistry* **2003**, *42*, 562.

(98) Best, R. B.; Clarke, J.; Karplus, M. *J. Mol. Biol.* **2005**, *349*, 185.

(99) Wand, A. J. *Nat. Struct. Biol.* **2001**, *8*, 926.

(100) Liu, W.; Flynn, P. F.; Fuentes, E. J.; Kranz, J. K.; McCormick, M.; Wand, A. J. *Biochemistry* **2001**, *40*, 14744.

(101) Walsh, S. T. R.; Lee, A. L.; DeGrado, W. F.; Wand, A. J. *Biochemistry* **2001**, *40*, 9560.

(102) Best, R. B.; Rutherford, T. J.; Freund, S. M.; Clarke, J. *Biochemistry* **2004**, *43*, 1145.

(103) Chou, J. J.; Case, D. A.; Bax, A. *J. Am. Chem. Soc.* **2003**, *125*, 8959.

(104) Hu, H.; Hermans, J.; Lee, A. L. *J. Biomol. NMR* **2005**, *32*, 151.

(105) Edgington, E. *Randomization Tests*, 3rd ed.; Marcel Dekker: New York, 1995.

(106) Lee, A. L.; Kinnear, S. A.; Wand, A. J. *Nat. Struct. Biol.* **2000**, *7*, 72.

(107) Ming, D. M.; Bruschweiler, R. *J. Biomol. NMR* **2004**, *29*, 363.

(108) Vugmeyster, L.; Trott, O.; McKnight, C. J.; Raleigh, D. P.; Palmer, A. G., 3rd. *J. Mol. Biol.* **2002**, *320*, 841.

(109) Cooper, A.; Dryden, D. T. F. *Eur. Biophys. J.* **1984**, *11*, 103.

(110) Hilser, V. J.; Dowdy, D.; Oas, T. G.; Freire, E. *Proc. Natl. Acad. Sci. U.S.A.* **1998**, *95*, 9903.

(111) Pan, H.; Lee, J. C.; Hilser, V. J. *Proc. Natl. Acad. Sci. U.S.A.* **2000**, *97*, 12020.

(112) Wand, A. J. *Science* **2001**, *293*, 1395.

(113) Wintrode, P. L.; Privalov, P. L. *J. Mol. Biol.* **1997**, *266*, 1050.

(114) Brokx, R. D.; Lopez, M. M.; Vogel, H. J.; Makhatadze, G. I. *J. Biol. Chem.* **2001**, *276*, 14083.

(115) Loh, A. P.; Pawley, N.; Nicholson, L. K.; Oswald, R. E. *Biochemistry* **2001**, *40*, 4590.

(116) Liu, T.; Whitten, S. T.; Hilser, V. J. *Proteins* **2006**, *62*, 728.

(117) Igumenova, T. I.; Lee, A. L.; Wand, A. J. *Biochemistry* **2005**, *44*, 12627.

(118) Goehlert, V. A.; Krupinska, E.; Regan, L.; Stone, M. J. *Protein Sci.* **2004**, *13*, 3322.

(119) Lockless, S. W.; Ranganathan, R. *Science* **1999**, *286*, 295.

(120) Hatley, M. E.; Lockless, S. W.; Gibson, S. K.; Gilman, A. G.; Ranganathan, R. *Proc. Natl. Acad. Sci. U.S.A.* **2003**, *100*, 14445.

(121) Suel, G. M.; Lockless, S. W.; Wall, M. A.; Ranganathan, R. *Nat. Struct. Biol.* **2003**, *10*, 59.

(122) Fuentes, E. J.; Der, C. J.; Lee, A. L. *J. Mol. Biol.* **2004**, *335*, 1105.

(123) Katoh, E.; Louis, J. M.; Yamazaki, T.; Gronenborn, A. M.; Torchia, D. A.; Ishima, R. *Protein Sci.* **2003**, *12*, 1376.

(124) Constantine, K. L.; Friedrichs, M. S.; Wittekind, M.; Jamil, H.; Chu, C. H.; Parker, R. A.; Goldfarb, V.; Mueller, L.; Farmer, B. T., 2nd. *Biochemistry* **1998**, *37*, 7965.

(125) Millet, O.; Mittermaier, A.; Baker, D.; Kay, L. E. *J. Mol. Biol.* **2003**, *329*, 551.

(126) Mittermaier, A.; Davidson, A. R.; Kay, L. E. *J. Am. Chem. Soc.* **2003**, *125*, 9004.

(127) Mittermaier, A.; Kay, L. E. *Protein Sci.* **2004**, *13*, 1088.

(128) Mittermaier, A.; Varani, L.; Muhandiram, D. R.; Kay, L. E.; Varani, G. *J. Mol. Biol.* **1999**, *294*, 967.

(129) Schnell, J. R.; Dyson, H. J.; Wright, P. E. *Biochemistry* **2004**, *43*, 374.

(130) Flynn, P. F.; Bieber Urbauer, R. J.; Zhang, H.; Lee, A. L.; Wand, A. J. *Biochemistry* **2001**, *40*, 6559.

(131) Kay, L. E.; Muhandiram, D. R.; Farrow, N. A.; Aubin, Y.; Forman-Kay, J. D. *Biochemistry* **1996**, *35*, 361.

(132) Finerty, P. J., Jr.; Mittermaier, A. K.; Muhandiram, R.; Kay, L. E.; Forman-Kay, J. D. *Biochemistry* **2005**, *44*, 694.

(133) Finerty, P. J., Jr.; Muhandiram, R.; Forman-Kay, J. D. *J. Mol. Biol.* **2002**, *322*, 605.

(134) Kay, L. E.; Muhandiram, D. R.; Wolf, G.; Shoelson, S. E.; Forman-Kay, J. D. *Nat. Struct. Biol.* **1998**, *5*, 156.

(135) Johnson, E. C.; Lazar, G. A.; Desjarlais, J. R.; Handel, T. M. *Struct. Folding Des.* **1999**, *7*, 967.

(136) Gagne, S. M.; Tsuda, S.; Spyracopoulos, L.; Kay, L. E.; Sykes, B. D. *J. Mol. Biol.* **1998**, *278*, 667.

(137) Chaykovski, M. M.; Bae, L. C.; Cheng, M. C.; Murray, J. H.; Tortolani, K. E.; Zhang, R.; Seshadri, K.; Findlay, J. H.; Hsieh, S. Y.; Kalverda, A. P.; Homans, S. W.; Brown, J. M. *J. Am. Chem. Soc.* **2003**, *125*, 15767.

(138) Hu, H.; Clarkson, M. W.; Hermans, J.; Lee, A. L. *Biochemistry* **2003**, *42*, 13856.

(139) Clarkson, M. W.; Lee, A. L. *Biochemistry* **2004**, *43*, 12448.

(140) Nicholls, A.; Sharp, K. A.; Honig, B. *Proteins* **1991**, *11*, 281.

(141) Meador, W. E.; Means, A. R.; Quiocho, F. A. *Science* **1992**, *257*, 1251.

(142) Koradi, R.; Billeter, M.; Wüthrich, K. *J. Mol. Graphics* **1996**, *14*, 51.